AD-A057 151 PENNSYLVANIA STATE UNIV UNIVERSITY PARK APPLIED RESE--ETC F/G 20/4
AN APPROXIMATE METHOD FOR CALCULATING THE MEAN STREAMLINES OF T--ETC(U)
MAY 78 M L BILLET
UNCLASSIFIED ARL/PSU/TM-78-161 N00017-73-C-1418
NL

1 OF 1
AD
A057 151

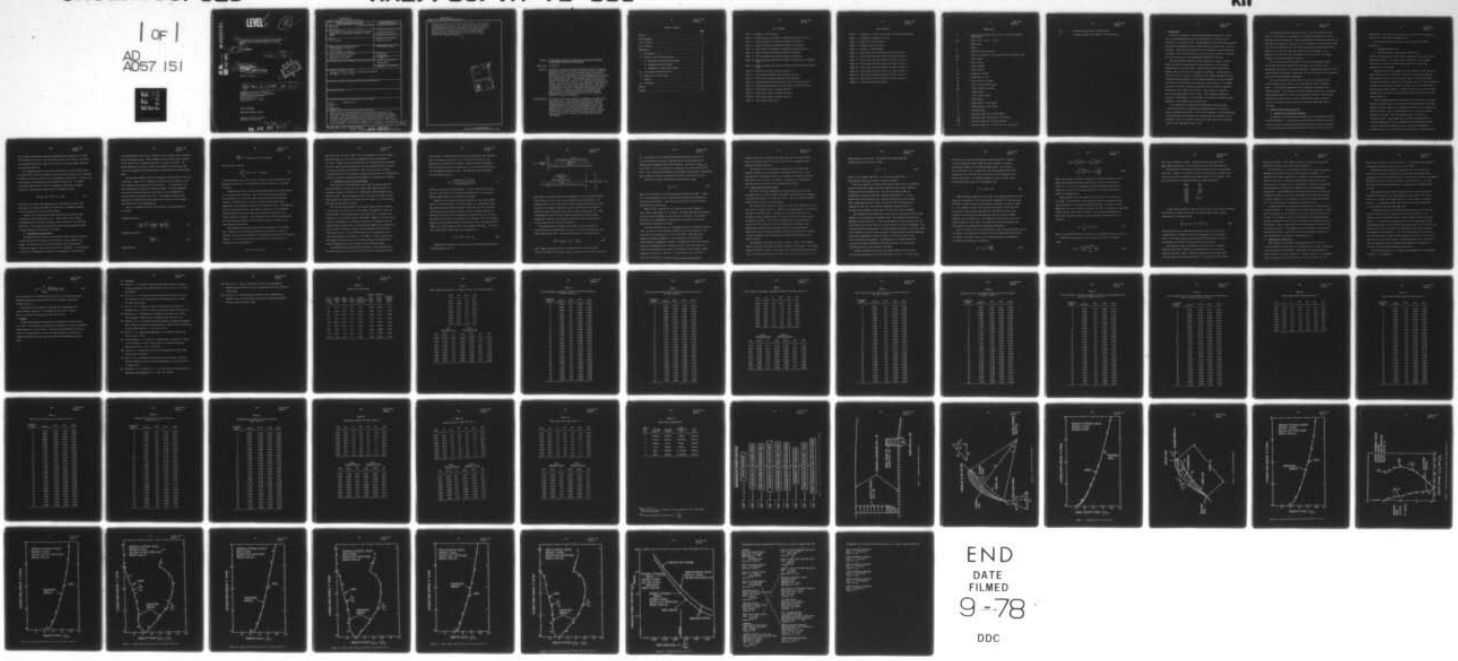

END
DATE
FILMED
9-78
DDC

LEVEL II

11

AN APPROXIMATE METHOD FOR CALCULATING THE MEAN STREAMLINES OF THE DIRECT PROBLEM OF AN OPEN ROTOR.

M. L. Billet

12 61 p.

Technical Memo.
File No. TM 78-161
11 May 1978
Contract N00017-73-C-1418

Copy No. 43

ARL/PSU/TM-78-161

The Pennsylvania State University
Institute for Science and Engineering
APPLIED RESEARCH LABORATORY
Post Office Box 30
State College, Pa. 16801

NAVY DEPARTMENT

NAVAL SEA SYSTEMS COMMAND

Approved for Public Release
Distribution Unlimited

UNCLASSIFIED

SECURITY CLASSIFICATION OF THIS PAGE (When Data Entered)

REPORT DOCUMENTATION PAGE		READ INSTRUCTIONS BEFORE COMPLETING FORM
1. REPORT NUMBER TM 78-161	2. GOVT ACCESSION NO.	3. RECIPIENT'S CATALOG NUMBER
4. TITLE (and Subtitle) AN APPROXIMATE METHOD FOR CALCULATING THE MEAN STREAMLINES OF THE DIRECT PROBLEM OF AN OPEN ROTOR		5. TYPE OF REPORT & PERIOD COVERED Technical Memorandum 6. PERFORMING ORG. REPORT NUMBER
7. AUTHOR(s) M. L. Billet		8. CONTRACT OR GRANT NUMBER(s) N00017-73-C-1418
9. PERFORMING ORGANIZATION NAME AND ADDRESS Applied Research Laboratory P. O. Box 30 State College, PA 16801		10. PROGRAM ELEMENT, PROJECT, TASK AREA & WORK UNIT NUMBERS
11. CONTROLLING OFFICE NAME AND ADDRESS Naval Sea Systems Command Washington, DC 20362		12. REPORT DATE 11 May 1978 13. NUMBER OF PAGES 58
14. MONITORING AGENCY NAME & ADDRESS(if different from Controlling Office)		15. SECURITY CLASS. (of this report) UNCLASSIFIED 15a. DECLASSIFICATION/DOWNGRADING SCHEDULE

16. DISTRIBUTION STATEMENT (of this Report)

Approved for Public Release. Distribution Unlimited.
Per NAVSEA - July 19, 1978.

17. DISTRIBUTION STATEMENT (of the abstract entered in Block 20, if different from Report)

18. SUPPLEMENTARY NOTES

19. KEY WORDS (Continue on reverse side if necessary and identify by block number)

rotor
streamline
flow
hydrodynamics
secondary flow

20. ABSTRACT (Continue on reverse side if necessary and identify by block number)

(U) As part of a program to analyze secondary flows in a rotor, an approximate method was utilized to obtain the mean streamlines through the rotor. The mean streamlines were calculated by means of an iterative procedure which simultaneously satisfies the principles of conservation of energy, momentum and continuity for incompressible flow. The procedure used to calculate the flow mean streamlines is a version of the streamline curvature method. For the direct method, it is necessary to determine the →

next page

DD FORM 1 JAN 73 1473 EDITION OF 1 NOV 65 IS OBSOLETE

UNCLASSIFIED

SECURITY CLASSIFICATION OF THIS PAGE (When Data Entered)

outlet flow angles for the rotor blade sections. This angle is a combination of the metal blade angle and a deviation angle. An approximate method for calculating this deviation angle is described which is based on available experimental data. A good correlation between predicted data and experimental measurements has been obtained using this direct analysis method for the mean streamlines.

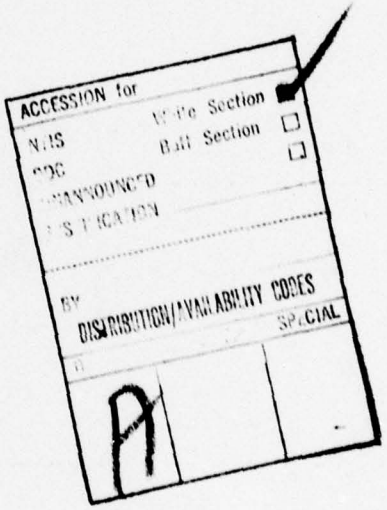

Subject: An Approximate Method for Calculating the Mean Streamlines of the Direct Problem of an Open Rotor

References: See page 25

Abstract: As part of a program to analyze secondary flows in a rotor, an approximate method was utilized to obtain the mean streamlines through the rotor. The mean streamlines were calculated by means of an iterative procedure which simultaneously satisfies the principles of conservation of energy, momentum and continuity for incompressible flow. The procedure used to calculate the flow mean streamlines is a version of the streamline curvature method. For the direct method, it is necessary to determine the outlet flow angles for the rotor blade sections. This angle is a combination of the metal blade angle and a deviation angle. An approximate method for calculating this deviation angle is described which is based on available experimental data. A good correlation between predicted data and experimental measurements has been obtained using this direct analysis method for the mean streamlines.

Acknowledgment: The results presented are part of a program on secondary flows in an open rotor. This research was carried out under the Naval Sea Systems Command General Hydromechanics Research Program Subproject SR 023 01 01, administered by the David W. Taylor Naval Ship Research and Development Center. The author would like to express his appreciation to Mr. Mark McBride whose streamline curvature program served as a basis for the direct problem solution and to Mr. Michael Pierzga who did the necessary computer program modifications and calculations.

Table of Contents

11 May 1978
MLB:jep

List of Tables

List of Figures

Nomenclature

a	- distance from leading edge of blade to point of maximum blade camber
AVR	- axial velocity ratio $\equiv V_{x_2}/V_{x_1}$
c	- blade chord
r	- radius
R'	- distance from body surface
R_m	- radius of curvature of the streamlines in meridional plane
R_R	- rotor radius
s	- blade spacing
t	- blade thickness
V_x	- axial velocity
V_θ	- tangential velocity
V_m	- meridional velocity
β_1	- inlet relative air angle
β_2	- outlet relative metal angle
β_2^*	- outlet relative air angle
λ	- stagger angle
ω	- rotor rotation speed
θ	- camber angle
$\varkappa_1$	- blade geometric inlet angle
$\varkappa_2$	- blade geometric outlet angle
δ	- deviation angle
δ_o	- deviation angle due to blade camber
δ_H	- deviation angle from Howell's correlation
$\Delta\delta^*$	- deviation angle due to blade thickness
$\Delta\delta'$	- deviation angle due to axial velocity acceleration

$\Delta\delta_s$ - deviation angle due to secondary flows

ϕ - streamline angle with respect to axial direction

I. Introduction

As part of a program to calculate the passage secondary flow for any rotor, an approximate method has been developed to calculate the mean streamlines of the primary flow. The primary flow is the calculated mean flow field which is axisymmetric and for cases discussed in this report is incompressible. The boundary conditions are (1) the geometry or metal angles of the blades, (2) the rpm of the rotor, (3) the velocity profile far upstream of the rotor plane and (4) the bounding streamlines of the flow.

This last boundary condition is most difficult to define. In most cases, the rotor is unique because of the uncertainty of the bounding stream-surface of the flow field. The flow field lacks a well-defined boundary such as the walls of a turbine or compressor. For this reason, the flow field for a rotor is considered to be a region constrained within a potential flow streamtube. The bounding streamsurface of this streamtube is actually located infinitely far from the rotor; however, it is assumed that there is a finite distance beyond which the flow field is relatively unaffected by the presence of the rotor. This distance is assumed to be at least eight times the rotor radius. This bounding streamsurface served as a flow boundary. In this manner, the bounding streamtube becomes analogous to the compressor and turbine walls.

It is important to realize that these boundary conditions imply a solution of the direct turbomachinery problem and not the indirect or design turbomachinery problem. For the direct problem, a rotor configuration is specified and the performance for any given initial conditions is to be calculated. Thus, the absolute blade outlet angle (α_2) must be specified instead of the tangential velocity (V_θ).

The equations which are commonly applied to calculate the mean streamlines of a flow field in an axisymmetric turbomachine comprise the so-called streamline curvature equations. These equations have been used for some time for the design and analysis of various types of turbomachines. As described by Novak [1], Frost [2], and Davis [3], this system of equations has been successfully applied for the indirect analysis of compressors and turbines. Also, McBride [4,5] has applied this streamline curvature method to the indirect problem of an open hydrodynamic propeller.

It is the objective of this paper to discuss an approximate method to calculate the mean streamlines for the direct rotor problem. This method uses the streamline curvature equations to establish the mean flow field for the boundary conditions. Comparisons are given between the calculated mean flow field and experimental measurements.

For the calculations in this paper, the rotor was located near the end of a large surface, and thus, the rotor operates within a boundary layer. The bounding streamline for this problem was determined in the following manner. The potential flow field was determined around an expanded surface which include the effects of displacement thickness. The bounding streamtube was then selected as that streamtube which passes through a circle in the plane of the rotor which has a radius eight times that of the rotor.

II. Method of Flow Field Calculation

A. Discussion of Calculation Procedure

A schematic of the calculation procedure for the final mean flow field is given in Figure 1. This outlines the iterative procedure for the calculation of the mean flow field and indicates the point at which refinements to the deviation angle are necessary and where secondary flow calculations

are employed. The final mean streamlines of the flow field consists of a coupling of the primary and secondary flows.

The initial conditions (Step 1) to the solution of the direct problem are:

1. bounding streamtube and
2. velocity profile in rotor plane without rotor.

With this information, the initial mean streamlines without rotor can be calculated (Step 2). The result of this calculation is the boundary condition of an initial velocity-energy profile of a station far upstream of the rotor plane.

Knowing the blade metal angles, the first estimate of the flow outlet angles (Step 3) can be calculated. These flow outlet angles depend on the blade metal angles and on a deviation angle. The deviation angle correlation developed by Howell [6] is initially applied. This relationship considers only thin blade sections and assumes that each blade section operates near design incidence. As shown in Figure 2, all of the boundary conditions are now known and the flow field can be solved with the rotor included (Step 4).

Once a converged solution is obtained for the mean flow field using Howell's deviation (Step 4), the axial velocity distributions are known whereby the inlet angles can be estimated in addition to the acceleration through the rotor. Now a second estimate of the rotor outlet angles (Step 5) can be made. For this deviation angle, the effects of acceleration ($\Delta\delta'$), blade camber (δ_o), and blade thickness ($\Delta\delta^*$) are calculated separately. For the calculation of the deviation term due to axial acceleration through the rotor, an equation developed by Lakshminarayana [7] is applied. For the calculation of deviation terms

due to camber and thickness effects, experimental data obtained by the staff of the National Aeronautics and Space Administration [8] are used. The result is an improved outlet flow angle profile which can be used to again calculate the flow field (Step 6).

The converged solution of the mean streamlines of the flow field (Step 6) is then used to solve the secondary vorticity equations (Step 7) and to determine a deviation term ($\Delta\delta_s$) which is due to nonsymmetric flow effects. The details of the secondary flow calculations are described in Billet [9]. An improved outlet flow angle profile (Step 8) is obtained by adding this secondary flow term to the deviation terms thus far calculated to obtain

$$\beta_2^* = \beta_2 - \Delta\delta' + \Delta\delta^* + \delta_o + \Delta\delta_s \quad , \tag{1}$$

where β_2^* is the outlet flow angle and β_2 is the blade metal outlet angle. This outlet flow angle distribution is then used as a boundary condition in the calculation of the flow field (Step 9).

Finally, all of the deviation angle calculations are checked based on the flow field calculated in Step 9. If the angles did not change significantly then the result obtained in Step 9 is used as the final mean flow field. If the angles were different, then these new angles were used to again calculate the final mean flow field.

B. Streamline Curvature Method

The major equations used in the streamline curvature method of analysis are derived from the principles of conservation of mass, momentum, and energy. In this analysis, the fluid is assumed to be incompressible, inviscid and steady. Because the flow field is axisymmetric, it is necessary to use only two components of velocity. One component of velocity which

is the meridional velocity (V_m) is tangent to the streamline and is projected onto the meridional plane. This component is related to the axial velocity by the cosine of the streamline angle (ϕ) to the axial direction. The second component of velocity is called the tangential velocity (V_θ), and is in the circumferential direction which is perpendicular to the meridional plane.

The resultant equations allow for streamline curvature and for vorticity in the flow. However, it is important to realize that the solution to the flow field does not contain all of the vorticity. In particular, only the circumferential vorticity is totally included. The other components of vorticity contain derivatives with respect to the circumferential direction which are assumed to be zero. As discussed by Hawthorne and Novak [10], the neglected vorticity terms can be related to the secondary flows that occur in the blade passage.

The set of equations used for this streamline curvature method are as follows:

r-momentum equation --

$$\frac{1}{\rho}\frac{\partial P}{\partial r} = \frac{V_\theta^2}{r} + V_m^2\left[\frac{\cos\phi}{R_m} - \frac{\sin\phi}{V_m}\frac{\partial V_m}{\partial m}\right] \tag{2}$$

θ-momentum equation --

$$\frac{\partial(rV_\theta)}{\partial\theta} = 0 \tag{3}$$

energy equation --

$$\frac{\partial(P_o)}{\partial m} = 0 \quad \text{(except across rotor plane)} \tag{4}$$

and continuity equation

$$2\pi \int_{r_1}^{r_2} V_m \cos\phi \cdot r dr = \text{constant} \quad . \tag{5}$$

In these equations, R_m is the radius of curvature of the streamlines in the meridional plane and ϕ is the streamlines angle with respect to the axial direction.

In Equation (2) there are three contributing factors in the development of the radial pressure gradient. The first term is directly related to the centrifugal force which the fluid experiences upon passing through the rotor. The second term is due to a moving fluid particle being subjected to the streamline curvature in the meridional plane. The magnitude of the term depends greatly on the radius of curvature of the streamline. The third term is due to the convective acceleration as the flow area either converges or diverges. The combination of these three terms defined the radial pressure gradient and the resultant equation is known as the radial equilibrium equation.

The computational procedure using the four equations is an iterative one. Initially, the velocity distribution at the reference station far upstream of the rotor is transferred to the downstream by using the continuity equation. At the rotor exit plane, the tangential velocity profile is related to the axial velocity by

$$V_\theta = \omega r - V_{x_2} \tan \beta_2^* \tag{6}$$

where β_2^* is the flow outlet angle. Now, the principle of constant angular momentum allows for the transfer of tangential velocity downstream of the rotor. Finally, the static pressure can be calculated along streamlines using the radial equilibrium equation and a new meridional velocity profile is calculated by using this pressure. This velocity-pressure coupling is repeated until the streamlines are located such that the flow simultaneously satisfies continuity, conservation of momentum, and conservation of energy.

C. Estimation of the Rotor Outlet Angles

The accuracy of the calculated velocity profiles depends primarily upon the prediction of the rotor exit angles (β_2^*) used in Equation (7). As shown in Figure 3, this angle is a combination of blade geometry and a deviation angle. The blade geometry outlet angle (β_2) is defined as the angle between the tangent to the blade section camber line at the trailing edge and the exit axial direction.

The correct determination of the deviation angle presents a problem. In particular, for the case of a rotor having a low hub-to-tip ratio and twisted blades, the deviation angle is more difficult to correlate even though the flow is turned through a small angle. However, the flow turning is still an expression of the guidance capacity of the passage formed by adjacent blade sections and it is expected that geometrical characteristics such as camber, thickness, solidity, and chord angle are the principle influencing factors. Thus, deviation angles can be estimated for each rotor radius based on the geometry of the blade. It can be expected that the largest errors will occur at the blade tip where three-dimensional factors dominate and at the root where viscous effects dominate.

From extensive cascade potential-flow theory, it was found that the deviation angle increases with blade camber and chord angle and decreases

with solidity. Using experimental results, investigators have correlated data to determine a deviation rule. In particular, Howell [6] has developed a correlation on the basis of nominal operating conditions. These cond'tions pertain to a deflection of the flow which is 80 percent of its maximum stalling deflection. This deviation angle is defined for each blade section as,

$$\delta_H \quad \frac{0.23(\theta_c)(s/c)^{1/2}(2a/c)^2}{1.0-(0.1/50)(\theta_c)(s/c)^{1/2}} \tag{7}$$

where θ_c is the section turning angle, s/c is the space-to-chord ratio, and a/c is the distance from the section leading edge to the point of maximum camber divided by the section chord length.

Equation (7) was used in the first estimate of rotor outlet angles (Step 4) in the calculation of the flow field. It is important to note that this deviation correlation assumes thin blades and that each blade section operates near design incidence. Once a converged solution is obtained for the flow field using Howell's deviation (Step 5), the inlet and outlet axial velocity distributions are estimated. Now, the deviation angle can be recalculated based on the effects of axial acceleration ($\Delta\delta'$), camber (δ_o), blade thickness ($\Delta\delta^*$), and secondary flows ($\Delta\delta_s$). Therefore, the second order deviation angle can be expressed as

$$\delta = \delta_o + \Delta\delta^* - \Delta\delta' + \Delta\delta_s \quad . \tag{8}$$

The deviation term due to acceleration in the blade passage is given by Lakshminarayana [7] as

$$\Delta\delta' = \frac{AVR-1.0}{AVR}\left\{\left\{\frac{\pi k(c/s)\left(\frac{G}{c}+\frac{\alpha}{4}\right)\cos\left(\frac{\beta_1+\beta_2}{2}\right)\left((AVR+1)^2-4\right)}{AVR-1.0}\right.\right.$$

$$\left.\left.\frac{}{8+\pi k\left(\frac{c}{s}\right)\left(\frac{\alpha}{4}+\frac{G}{c}\right)\cos\left(\frac{\beta_1+\beta_2}{2}\right)\left((AVR+1)\tan\beta_2+2\tan\beta_1\right)}\right.$$

$$\left.\left.-\frac{\frac{2\pi k\left(\frac{c}{s}\right)\tan\beta_1}{AVR\cos\left(\frac{\beta_1+\beta_2}{2}\right)\sec^2\beta_1}}{8+\pi k\left(\frac{c}{s}\right)\left(\frac{\alpha}{4}+\frac{G}{c}\right)\cos\left(\frac{\beta_1+\beta_2}{2}\right)\left((AVR+1)\tan\beta_2+2\tan\beta_1\right)}\right\}+\tan\beta_2\right\}\cos^2\beta_2 \quad (9)$$

where AVR is the axial velocity ratio (V_{x_2}/V_{x_1}), k is the cascade influence coefficient, G/c is the ratio of the distance from the chordline to the maximum camber point of the section to chord length, β_1 and β_2 are the inlet and outlet flow angles, respectively, and α is defined as the difference between the inlet flow angle (β_1) and the section stagger angle (λ). This relationship is valid for small changes in AVR and for small turning. Perhaps most important, the deviation angle due to axial acceleration in the flow always reduces the total deviation.

The deviation due to thickness and camber is given by empirical data which have been obtained by the staff of the National Aeronautics and Space Administration [8]. The thickness deviation is calculated from

$$\Delta\delta^* = (k_\delta)_{sh} \cdot (k_\delta)_t \cdot (\delta_o^o)_{10} \quad . \quad (10)$$

where $(\delta_o^o)_{10}$ represents the basic variation for the 10-percent thick 65-series thickness distribution, $(k_\delta)_{sh}$ represents any correction necessary

for a blade shape with a thickness distribution different from that of the 65-series blade, and $(k_\delta)_t$ represents any correction necessary for maximum blade thicknesses other than 10 percent. The value of $(k_\delta)_{sh}$ can range from 1.1 to 0.7; therefore, an average value of 0.9 was used for the rotor. Also, the other coefficients are determined from graphs of experimental data in Reference [8] for given values of solidity and inlet flow angle.

The effect of camber on deviation is calculated by using

$$\delta_o = m\,\theta_c \tag{11}$$

where m is the slope of the deviation angle variation with camber. Values of m can be determined from the figures given in NASA [8] by knowing the inlet angle and solidity. This slope can be found for both circular-arc and parabolic-arc mean lines.

Equations (9), (10) and (11) are used for the second estimate of rotor outlet angles (Step 5). In order to use these deviation relationships the axial velocity through the rotor had to be estimated. This velocity estimation was accomplished by using Howell's correlation in the first calculation of the mean flow field.

The last deviation term to be considered is due to the passage secondary flow. The effect of this passage secondary flow is most dramatic in the exit plane of the blades near the rotor inner wall. Secondary flows produce a streamwise component of vorticity which is not taken into consideration by axisymmetric analysis. The means by which this streamwise vorticity is produced in this relative flow for a rotor are similar to those in a stationary system, namely, the turning of flow having a normal component of vorticity. However, it is important to note that when solving for the flow in a relative reference frame that additional

secondary vorticity is generated when the cross product of the rotation vector ($\vec{\Omega}$) and the relative velocity vector ($\vec{W}$) has a component in the relative streamwise direction.

The solution for the streamwise secondary vorticity involves the numerical solution of two equations as discussed by Billet [9]. After calculating the streamwise vorticity, a secondary stream function solution was found in the exit plane of the rotor. The results are perturbation velocities which are used to find a deviation angle ($\Delta\delta_s$).

III. Initial Flow Field Calculation

The case of the rotor operating near design (Basic Flow No. 1) was calculated first in order to obtain some general results about the influence of the deviation angle on the mean flow field. The rotor operated within a boundary layer created by a large surface.

The boundary layer profile in the plane of the rotor without the rotor on the surface is shown in Figure 4. Details of the measurements of this profile are given in Reference [10]. The profile was extended upstream by the streamline curvature method (Step 2) in order to obtain a velocity profile far upstream of rotor. This profile is needed for a boundary condition of the flow field; however, it does not agree with the boundary layer profile which would exist on the surface at this far upstream point. A comparison between the measured profile and the calculated profile obtained at this measurement plane by using the aforementioned procedure is also shown in Figure 4.

The geometry of the rotor is given in Table 1. Most of the loading occurs at the mid-radius where the camber angles are the largest. The stagger angels are high as a result of the design flow coefficient being approximately 0.30. The blade sections are very thick near the inner wall which can cause

large deviations in the flow. The metal outlet angles (β_2) were determined from the geometry by using

$$\beta_2 = \lambda - \chi_2 \tag{12}$$

where λ is the stagger angle and χ_2 is the outlet camber angle. A description of the various angles is shown in Figure 5.

The first estimate of the flow outlet angles (Step 3) can be calculated using the blade metal angles (β_2) and a deviation angle based on Howell's correlation given by Equation (7). The outlet flow angles (β_2^*) are determined by using the streamline curvature method (Step 4). In all, twenty-eight mean streamlines were calculated through the rotor with the first streamline being at the inner wall and the last streamline going through the rotor tip. The velocity components are given in Table 3 for each inlet streamline and in Table 4 for the same outlet streamline.

The streamlines were spaced more closely near the inner wall because of the emphasis on the caculation of secondary flows. The secondary flows are most important near the inner wall. Also, the streamline curvature equations are for an inviscid fluid so that there is a finite velocity at the wall streamline. The solution shows an acceleration of the axial velocity along most of the mean streamlines. However, the flow characteristics at a constant radius are more meaningful. The velocity components are given in Table 2 for the radii used in the outlet flow angle calculations. A comparison shows a large acceleration of the axial velocity through the rotor with the exception of the rotor tip where the flow is most difficult to define.

A better estimate of the outlet flow angles (Step 5) for this rotor can be made using the mean flow field calculated in Step 4. The inlet flow

flow angles (β_1) and the axial velocity ratios (AVR) can be computed so that a method developed by NASA [8] can be applied to estimate the deviation angles for any blade incidence angle. The effects of axial acceleration ($\Delta\delta'$), camber (δ_o), and blade thickness ($\Delta\delta^*$) given by Equations (9), (10) and (11) respectively, were calculated for the primary blade radii. The deviation angles are given in Table 5 where the total deviation angle (δ) is determined from

$$\delta = \delta_o + \Delta\delta^* - \Delta\delta' \quad . \tag{14}$$

These new outlet angles were then used in the second calculation of the mean flow field (Step 6). The inlet velocity components for each streamline are given in Table 6 and the outlet velocity components are given in Table 7. It is important to note that the major differences in the flow field as compared to the solution using Howell's correlation are due to the effects of acceleration near the mid-radius and the effects of blade thickness near the blade root. The tangential velocity near the root was reduced primarily by the effect of thickness and the axial velocity near the mid-radius was increased by including the AVR effect.

From the primary mean flow field analysis using the second estimate of outlet angles, the streamlines through the rotor are again determined (Step 6). The effect of secondary flows can be calculated along these streamlines by using the following set of equations

$$\omega_n' = \omega_{n_1}' \cdot \frac{W_1 \, ab_1'}{W \, a_b'} \tag{15}$$

$$\omega_{s_2}' = W_2 \int_1^2 \frac{2\,\omega_n'}{W\,R'}\,ds' + W_2 \int_1^2 \frac{2\,\Omega_b'\,\omega_n'}{W^2}\,ds'$$

$$- W_2 \int_1^2 \frac{2\,\Omega_n'\,\omega_b'}{W^2}\,ds' + \omega_{s_1}' \left\{\frac{W_2}{W_1}\right\} \qquad (16)$$

where ω_n' and ω_s' are the relative components of absolute vorticity in the normal and streamwise direction respectively, Ω is the rotor rotation vector, s', n', b' are the streamwise, normal and bi-normal directions respectively, and W is the relative velocity. All other definitions are found in the nomenclature.

These equations give the change in vorticity due to the presence of the blades. The difference in the streamwise vorticity between the rotor inlet and outlet is the passage secondary vorticity. The effect of this additional vorticity is found on the mean flow field by solving for a secondary stream function in the rotor exit plane. As discussed by Hawthorne and Novak [10]; the series solution for the secondary stream function is in the form

$$\Psi_s = \sum_{1,3\ldots}^{\infty} \Psi_n \sin n\pi\theta \qquad (17)$$

where Ψ_n are determined from the solution of the equation in the r-direction.

The deviation angle due to the secondary flows can be calculated using

$$\Delta\delta_s = -\frac{N \cos^2 \beta_2^*}{2\pi\, V_x} \int_0^{2\pi/N} \frac{\partial\Psi}{\partial r}\,d\theta \qquad (18)$$

where N is the number of blades. The axial velocity (V_x) and outlet angle (β_2^*) are determined in the calculation of the flow field (Step 6).

The details of the secondary flow calculations will not be discussed in this report. However, the results indicate that the effects are significant only near the blade root where the incoming vorticity is the largest. This can be seen from the following tabulation of angle deviations:

R'/R_R	$\Delta\delta'_s$
0.00	-5.4°
0.04	-2.9°
0.14	-1.0°
0.24	
0.34	
0.44	<0.2°
0.54	
0.64	

A third calculation of the mean flow field (Step 9) was found by including the effects of secondary flows with the previous NASA deviation angles. The angles were calculated using

$$\beta_2^* = \beta_2 + \delta_o - \Delta\delta' + \Delta\delta^* + \Delta\delta_s \quad . \tag{19}$$

The resulting velocity components are given in Table 8 for the inlet streamlines and in Table 9 for the same streamlines in the rotor exit plane. The primary effects of the secondary flow deviation are seen in the increase of tangential velocities near the inner wall.

Each deviation angle contribution was calculated for a slightly different flow field. Therefore, a check was made on the effects of axial acceleration, camber, and blade thickness on the deviation angle using the flow field calculated in Step 9. The resulting outlet angles

are given in Table 9. They compare closely to the previous calculation without the secondary flow effects given in Table 5.

The final mean flow field is given in Table 11 for the inlet velocity components and in Table 12 for the outlet velocity components. In addition, the velocity components at a station one chord length upstream of rotor inlet and at a station one chord length downstream of rotor outlet are given in Table 13 and 14 respectively. These profiles upstream and downstream of the rotor can be compared to previous experimental measurements. The measurements are discussed in References [11] and [12]. A comparison between the calculated and measured inlet velocity profiles is shown in Figure 6. The comparison is quite good except near the wall where the inviscid theory over-predicts the axial velocity.

A comparison with the calculated and measured rotor outlet profiles is shown in Figure 7. The agreement in the axial velocity profile is quite good including the effect of the rotor tip shown by the dip in the axial velocity. The tangential velocity profiles are also in good agreement. The major difference is near the rotor tip where three-dimensional effects are dominate. Near the inner wall, the calculated profile is fuller than the measured profile. This difference can be attributed to the inviscid secondary flow theory. Near the inner wall the secondary vorticity is over-predicted due to the lack of a dissipative term.

IV. Application to Other Flows

This calculation procedure for determining the flow field for a rotor was applied to other basic flow configurations for which experimental velocity profiles were available. These basic flow configurations or Basic Flow Nos. are given in Table 18. For Basic Flow No. 4, the upstream struts consisted of four struts placed at the 0°, 90°, 180° and 270°

points on the surface in front of the rotor. The upstream screen consisted of placing a two foot section of screen on the surface.

The boundary layer profiles in the plane of the rotor without the rotor used in the initial calculation for each case were obtained from experimental results (see Reference [11]). All of the cases had an axisymmetric boundary layer profile with the exception of Basic Flow No. 4. For this case which had four upstream struts, a circumferentially averaged profile was used.

The outlet flow angles were determined for each case by the method outlined in this report. The final angles are given in Table 15 for Basic Flow No. 2, in Table 16 for Basic Flow No. 3, and in Table 17 for Basic Flow No. 4. A comparison between cases show that the large differences in outlet angles occur near the blade root.

A comparison between the calculated and experimental rotor inlet and outlet profiles is made in Figures 8 and 9 for Basic Flow No. 2, in Figures 10 and 11 for Basic Flow No. 3, and in Figures 12 and 13 for Basic Flow No. 4. In general, the calculations are in good agreement with the experimental results. The calculated mean axial velocity near the inner wall for the outlet flow is less than the experimental value which is typical of secondary flow predictions. Also, the calculated inlet axial velocity near the inner wall is higher than the measured value for all of the cases. This is due to the inviscid theory. Comparisons between basic flows show that the tangential velocity increased significantly by operating at a low flow coefficient and by adding upstream struts.

The torque coefficient is a measure of the magnitude of the tangential velocity. It is defined as

$$C_Q = 2\pi \int_{R_I/R_R}^{1} \left(\frac{V_\theta}{V_\infty}\right)\left(\frac{V_m}{V_\infty}\right)\left(\frac{r}{R_R}\right) d\left(\frac{r}{R_R}\right) \quad . \tag{20}$$

This coefficient was calculated from the flow field for each case and was normalized by the coefficient obtained from the reference case which is Basic Flow No. 1.

These results were compared to experimentally determined torque curve as shown in Figure 14. The changes in torque due to adding struts or operating off design are predicted very well.

V. Summary

An approximate method is presented for analyzing the mean flow field of a rotor. In particular, this method was developed for a study in secondary flows produced in a rotor passage. The mean streamline method is not new; however, the application to an open rotor demonstrates its versatility. Comparisons between the final mean flow field and measurements are quite good.

VI. References

[1] Novak, R. A., "Streamline Curvature Computing Procedures," Journal of Engr. for Power, Trans. ASME, Series A, Vol. 89, No. 4, Oct. 1967, pp. 478-490.

[2] Frost, D. H., "A Streamline Curvature Through-Flow Computer Program for Analyzing the Flow Through Axial Flow Turbomachines," ARC R&M No. 3687, August 1970.

[3] Davis, W. R., "A Computer Program for the Analysis and Design of Turbomachinery -- Revison," Carleton University, Report No. ME/A 71-5.

[4] McBride, M. W., "Refinement of the Mean Streamline Method of Blade Section Design," ASME Paper No. 76-WA/FE11, New York, New York.

[5] McBride, M. W., "A Streamline Curvature Method of Analyzing Axisymmetric Axial, Mixed and Radial Flow Turbomachinery," Applied Research Laboratory, Technical Memorandum No. 77-219, 21 July 1977.

[6] Horlock, J. H., Axial Flow Compressors, R. E. Krieger Company, New York, 1973, pp. 55-60.

[7] Lakshminarayana, B., Discussion of Wilson, Mani, and Acosta's, "A Note on the Influence of Axial Velocity Ratios on Cascade Performance," NASA SP-304, Part 1, 1974, pp. 127-133.

[8] Lieblein, S., "Experimental Flow in Two-Dimensional Cascades," NASA SP-36, 1965, pp. 209-222.

[9] Billet, M. L., "Secondary Flow Vorticity in the Passage of a Rotor," Applied Research Laboratory Technical Memorandum, File No. TM 77-243, 17 August 1977.

[10] Hawthorne, W. R. and Novak, R. A., "The Aerodynamics of Turbo-Machinery," Ann. Rev. Fluid Mechanics, Vol. 1, 1969, pp. 341-366.

[11] Billet, M. L., "Rotor Incoming Velocity Profile Measurements," Applied Research Laboratory Technical Memorandum, File No. TM 76-254, October 1976.

[12] Billet, M. L., "Flow Measurements Behind a Rotor Operating in a Boundary Layer," Applied Research Laboratory Technical Memorandum, File No. TM 76-260, October 1976.

Table 1

Geometry of Rotor Blades

Blade Section (r/R_R)	Stagger Angle (λ)	Camber Angle (θ)	Exit Angle ($\varkappa_2$)	Metal Outlet Angle ($\beta_2=\lambda-\varkappa_2$)	Space to Chord Ratio (s/c)	Thickness to Chord Ratio (t/c)	Point of Maximum Camber (a/c)
0.2	51.3	7.8	3.8	47.5	0.63	0.28	0.52
0.3	55.8	12.2	6.0	49.8	0.82	0.21	0.53
0.4	59.8	14.3	7.1	52.7	0.98	0.16	0.48
0.5	63.3	14.7	7.4	55.9	1.14	0.12	0.47
0.6	66.6	14.3	7.0	59.6	1.33	0.10	0.49
0.7	69.2	11.8	5.7	63.5	1.55	0.082	0.49
0.8	71.6	9.0	4.4	67.2	1.88	0.068	0.49
0.9	73.0	5.7	2.8	70.2	2.53	0.059	0.47
0.95	75.0	2.9	1.7	73.3	3.44	0.056	0.47

Table 2

Outlet Angles Using Howell's Correlation (Step 4) for Basic Flow No. 1

r/R_R	β_2	δ_H	β_2^*
0.26	49.0	3.0	52.0
0.30	49.8	4.0	53.8
0.40	52.7	4.6	57.3
0.50	55.9	5.1	61.0
0.60	59.6	5.8	65.4
0.70	63.5	5.3	68.8
0.80	67.2	4.5	71.7
0.90	70.2	3.1	73.3
0.95	73.3	1.9	75.2

	Inlet Velocity Profile		Outlet Velocity Profile			
r/R_R	V_x/V_∞	β_1	V_x/V_∞	V_θ/V_∞	β_2^*	AVR
0.26	0.401	65.8	0.489	0.260	52.3	1.217
0.30	0.509	63.7	0.569	0.254	53.8	1.117
0.40	0.631	65.3	0.719	0.249	57.4	1.139
0.50	0.706	67.7	0.828	0.229	60.9	1.172
0.60	0.764	69.7	0.861	0.175	65.5	1.127
0.70	0.812	71.4	0.886	0.129	68.8	1.091
0.80	0.841	73.0	0.895	0.087	71.4	1.064
0.90	0.864	74.4	0.916	0.055	73.2	1.061
0.95	0.872	75.1	0.854	0.021	75.2	0.979

Table 3

Inlet Streamline Data Based on Howell's Correlation (Step 4)
for Basic Flow No. 1

Streamline Number	r (inches)	V_θ/V_∞	V_x/V_∞	V_m/V_∞
1	0.974	0.0	0.401	0.416
2	0.998	0.0	0.422	0.436
3	1.020	0.0	0.439	0.453
4	1.041	0.0	0.455	0.468
5	1.061	0.0	0.469	0.483
6	1.080	0.0	0.483	0.496
7	1.150	0.0	0.521	0.533
8	1.211	0.0	0.545	0.557
9	1.268	0.0	0.567	0.578
10	1.320	0.0	0.585	0.596
11	1.368	0.0	0.599	0.610
12	1.530	0.0	0.638	0.650
13	1.670	0.0	0.666	0.678
14	1.794	0.0	0.690	0.704
15	1.906	0.0	0.712	0.727
16	2.009	0.0	0.729	0.745
17	2.196	0.0	0.756	0.774
18	2.362	0.0	0.779	0.799
19	2.514	0.0	0.800	0.821
20	2.653	0.0	0.814	0.836
21	2.784	0.0	0.825	0.848
22	2.986	0.0	0.840	0.865
23	3.172	0.0	0.853	0.878
24	3.346	0.0	0.862	0.888
25	3.509	0.0	0.870	0.894
26	3.664	0.0	0.876	0.899
27	3.811	0.0	0.884	0.905
28	3.952	0.0	0.893	0.911

Table 4

Outlet Streamline Data Based on Howell's Correlation (Step 4)
for Basic Flow No. 1

Streamline Number	r (inches)	V_θ/V_∞	V_x/V_∞	V_m/V_∞
1	0.796	0.292	0.359	0.371
2	0.827	0.285	0.385	0.397
3	0.857	0.279	0.407	0.419
4	0.884	0.274	0.427	0.438
5	0.908	0.269	0.445	0.456
6	0.931	0.266	0.461	0.472
7	1.013	0.258	0.512	0.522
8	1.082	0.255	0.548	0.558
9	1.144	0.253	0.579	0.588
10	1.199	0.252	0.604	0.614
11	1.251	0.251	0.627	0.636
12	1.416	0.250	0.691	0.700
13	1.553	0.249	0.738	0.748
14	1.671	0.245	0.776	0.787
15	1.777	0.238	0.806	0.818
16	1.875	0.229	0.828	0.841
17	2.051	0.206	0.849	0.865
18	2.210	0.181	0.859	0.875
19	2.357	0.160	0.868	0.885
20	2.494	0.144	0.878	0.897
21	2.622	0.130	0.886	0.905
22	2.822	0.106	0.889	0.910
23	3.008	0.086	0.896	0.918
24	3.180	0.074	0.916	0.938
25	3.342	0.059	0.919	0.942
26	3.499	0.035	0.884	0.904
27	3.658	0.005	0.817	0.835
28	3.814	0.000	0.832	0.847

Table 5

Outlet Angles Using NASA's Correlation (Step 5) for Basic Flow No. 1

r/R_R	β_2	δ_o	$\Delta\delta^*$	$\Delta\delta'$	β_2^*
0.26	49.0	2.6	10.1	4.5	57.2
0.30	49.8	3.5	6.9	2.2	58.0
0.40	52.7	4.6	4.2	2.5	59.0
0.50	55.9	5.4	2.5	2.9	60.9
0.60	59.6	5.7	1.7	2.0	65.0
0.70	63.5	5.1	1.3	1.4	68.5
0.80	67.2	4.4	0.7	0.9	71.4
0.90	70.2	3.2	0.6	0.8	73.2
0.95	73.3	1.5	0.3	0.0	75.1

	Inlet Velocity Profile		Outlet Velocity Profile			
r/R_R	V_x/V_∞	β_1	V_x/V_∞	V_θ/V_∞	β_2^*	AVR
0.26	0.370	67.5	0.432	0.215	57.5	1.167
0.30	0.483	64.9	0.516	0.209	57.9	1.069
0.40	0.618	65.8	0.692	0.224	58.9	1.120
0.50	0.704	67.8	0.831	0.229	60.9	1.181
0.60	0.768	69.6	0.877	0.185	64.9	1.148
0.70	0.818	71.3	0.905	0.139	68.3	1.107
0.80	0.845	72.9	0.899	0.090	71.3	1.063
0.90	0.867	74.4	0.921	0.058	73.1	1.063
0.95	0.874	75.0	0.860	0.024	75.1	0.984

Table 6

Inlet Streamline Data Based on NASA's Correlation (Step 6)
for Basic Flow No. 1

Streamline Number	r (inches)	V_θ/V_∞	V_x/V_∞	V_m/V_∞
1	0.974	0.0	0.370	0.383
2	1.000	0.0	0.393	0.405
3	1.024	0.0	0.412	0.424
4	1.046	0.0	0.428	0.411
5	1.066	0.0	0.444	0.456
6	1.087	0.0	0.459	0.470
7	1.159	0.0	0.510	0.500
8	1.222	0.0	0.536	0.527
9	1.280	0.0	0.550	0.559
10	1.333	0.0	0.569	0.578
11	1.382	0.0	0.586	0.594
12	1.546	0.0	0.630	0.639
13	1.686	0.0	0.662	0.671
14	1.809	0.0	0.689	0.699
15	1.921	0.0	0.713	0.725
16	2.023	0.0	0.732	0.746
17	2.207	0.0	0.762	0.777
18	2.371	0.0	0.786	0.804
19	2.521	0.0	0.806	0.826
20	2.659	0.0	0.820	0.842
21	2.788	0.0	0.381	0.853
22	2.989	0.0	0.845	0.869
23	3.174	0.0	0.857	0.882
24	3.347	0.0	0.866	0.891
25	3.510	0.0	0.872	0.897
26	3.665	0.0	0.878	0.902
27	3.812	0.0	0.886	0.907
28	3.952	0.0	0.894	0.913

Table 7

Outlet Streamline Data Based on NASA's Correlation (Step 6)
for Basic Flow No. 1

Streamline Number	r (inches)	V_θ/V_∞	V_x/V_∞	V_m/V_∞
1	0.796	0.251	0.311	0.321
2	0.832	0.241	0.338	0.348
3	0.865	0.234	0.361	0.370
4	0.895	0.227	0.381	0.390
5	0.922	0.223	0.399	0.408
6	0.947	0.218	0.416	0.424
7	1.036	0.210	0.468	0.476
8	1.109	0.209	0.508	0.516
9	1.173	0.208	0.542	0.549
10	1.231	0.209	0.571	0.577
11	1.284	0.211	0.596	0.603
12	1.451	0.221	0.673	0.679
13	1.587	0.230	0.730	0.738
14	1.704	0.234	0.777	0.785
15	1.807	0.233	0.812	0.822
16	1.902	0.228	0.837	0.848
17	2.074	0.209	0.863	0.876
18	2.229	0.187	0.875	0.890
19	2.372	0.169	0.887	0.904
20	2.505	0.154	0.899	0.917
21	2.630	0.139	0.905	0.925
22	2.826	0.111	0.900	0.921
23	3.010	0.089	0.900	0.922
24	3.182	0.076	0.818	0.941
25	3.343	0.062	0.924	0.947
26	3.499	0.037	0.889	0.911
27	3.656	0.007	0.824	0.841
28	3.813	0.000	0.831	0.846

Table 8

Inlet Streamline Data Based on NASA's Correlation with Secondary Flows (Step 8) for Basic Flow No. 1

Streamline Number	r (inches)	V_θ/V_∞	V_x/V_∞	V_m/V_∞
1	0.974	0.0	0.410	0.424
2	0.998	0.0	0.429	0.443
3	1.019	0.0	0.445	0.460
4	1.040	0.0	0.460	0.475
5	1.060	0.0	0.473	0.488
6	1.079	0.0	0.485	0.500
7	1.148	0.0	0.521	0.535
8	1.210	0.0	0.543	0.557
9	1.267	0.0	0.564	0.577
10	1.319	0.0	0.582	0.594
11	1.368	0.0	0.596	0.608
12	1.531	0.0	0.636	0.647
13	1.671	0.0	0.664	0.676
14	1.796	0.0	0.689	0.702
15	1.908	0.0	0.711	0.726
16	2.011	0.0	0.728	0.744
17	2.198	0.0	0.755	0.773
18	2.364	0.0	0.777	0.797
19	2.516	0.0	0.796	0.818
20	2.656	0.0	0.809	0.832
21	2.788	0.0	0.819	0.843
22	2.990	0.0	0.835	0.859
23	3.178	0.0	0.848	0.873
24	3.352	0.0	0.858	0.883
25	3.516	0.0	0.867	0.890
26	3.670	0.0	0.875	0.897
27	3.818	0.0	0.884	0.904
28	3.959	0.0	0.894	0.912

Table 9

Outlet Streamline Data Based on NASA's Correlation with Secondary Flows (Step 8) for Basic Flow No. 1

Streamline Number	r (inches)	V_θ/V_∞	V_x/V_∞	V_m/V_∞
1	0.796	0.366	0.431	0.446
2	0.823	0.357	0.452	0.466
3	0.848	0.349	0.469	0.483
4	0.872	0.341	0.483	0.497
5	0.894	0.332	0.495	0.509
6	0.915	0.323	0.506	0.519
7	0.993	0.291	0.532	0.544
8	1.063	0.265	0.542	0.554
9	1.127	0.244	0.552	0.563
10	1.188	0.232	0.567	0.576
11	1.242	0.227	0.585	0.594
12	1.416	0.234	0.667	0.677
13	1.556	0.246	0.736	0.747
14	1.674	0.247	0.782	0.793
15	1.779	0.241	0.811	0.824
16	1.876	0.231	0.831	0.844
17	2.051	0.206	0.850	0.865
18	2.210	0.180	0.859	0.875
19	2.358	0.159	0.868	0.886
20	2.495	0.143	0.878	0.897
21	2.623	0.127	0.883	0.903
22	2.825	0.099	0.877	0.898
23	3.013	0.078	0.878	0.899
24	3.189	0.066	0.898	0.919
25	3.353	0.053	0.906	0.928
26	3.510	0.032	0.880	0.900
27	3.668	0.008	0.830	0.847
28	3.823	0.000	0.834	0.849

Table 10

Final Outlet Angles for Basic Flow No. 1

r/R_R	β_2	δ_o	$\Delta\delta^*$	$\Delta\delta'$	$\Delta\delta_s$	β_2^*
0.26	49.0	2.5	12.2	3.3	-5.3	55.1
0.30	49.8	3.6	7.2	2.1	-2.9	55.6
0.40	52.7	4.7	4.0	2.3	-0.9	58.2
0.50	55.9	5.4	2.4	2.9	0.0	60.8
0.60	59.6	5.8	1.7	2.2	0.0	64.9
0.70	63.5	5.2	1.2	1.6	0.0	68.3
0.80	67.2	4.5	0.8	0.8	0.0	71.7
0.90	70.2	3.2	0.6	1.0	0.0	73.0
0.95	73.3	1.8	0.0	0.0	0.0	75.1

Table 11

Final Inlet Streamline Data for Basic Flow No. 1

Streamline Number	r (inches)	V_θ/V_∞	V_x/V_∞	V_m/V_∞
1	0.974	0.0	0.387	0.400
2	0.998	0.0	0.408	0.421
3	1.021	0.0	0.426	0.439
4	1.043	0.0	0.443	0.455
5	1.063	0.0	0.458	0.470
6	1.083	0.0	0.472	0.484
7	1.154	0.0	0.512	0.523
8	1.216	0.0	0.537	0.547
9	1.273	0.0	0.560	0.570
10	1.325	0.0	0.578	0.588
11	1.374	0.0	0.593	0.603
12	1.537	0.0	0.635	0.646
13	1.677	0.0	0.665	0.676
14	1.800	0.0	0.691	0.703
15	1.912	0.0	0.715	0.728
16	2.014	0.0	0.733	0.748
17	2.199	0.0	0.762	0.779
18	2.364	0.0	0.786	0.804
19	2.514	0.0	0.806	0.827
20	2.652	0.0	0.819	0.842
21	2.783	0.0	0.829	0.853
22	2.984	0.0	0.843	0.868
23	3.169	0.0	0.855	0.881
24	3.343	0.0	0.864	0.889
25	3.506	0.0	0.870	0.895
26	3.662	0.0	0.877	0.900
27	3.809	0.0	0.884	0.906
28	3.950	0.0	0.894	0.912

Table 12

Final Outlet Streamline Data for Basic Flow No. 1

Streamline Number	r (inches)	V_θ/V_∞	V_x/V_∞	V_m/V_∞
1	0.796	0.267	0.330	0.341
2	0.830	0.259	0.357	0.368
3	0.861	0.252	0.380	0.391
4	0.890	0.247	0.400	0.411
5	0.915	0.243	0.419	0.429
6	0.940	0.239	0.436	0.446
7	1.024	0.233	0.490	0.499
8	1.097	0.233	0.531	0.540
9	1.159	0.233	0.565	0.573
10	1.215	0.233	0.592	0.600
11	1.267	0.234	0.614	0.623
12	1.432	0.235	0.680	0.688
13	1.569	0.237	0.730	0.739
14	1.688	0.238	0.774	0.784
15	1.792	0.236	0.810	0.821
16	1.888	0.232	0.836	0.848
17	2.062	0.212	0.862	0.876
18	2.218	0.189	0.874	0.889
19	2.361	0.171	0.887	0.905
20	2.495	0.156	0.901	0.919
21	2.621	0.140	0.905	0.925
22	2.818	0.107	0.889	0.910
23	3.006	0.083	0.881	0.903
24	3.179	0.075	0.913	0.937
25	3.340	0.065	0.933	0.957
26	3.495	0.039	0.897	0.919
27	3.653	0.005	0.816	0.834
28	3.810	0.000	0.830	0.846

Table 13

Streamline Data Upstream of Rotor Inlet for
Basic Flow No. 1

Streamline Number	r (inches)	V_θ/V_∞	V_x/V_∞	V_m/V_∞
1	1.238	0.0	0.372	0.387
2	1.259	0.0	0.391	0.407
3	1.278	0.0	0.408	0.424
4	1.296	0.0	0.423	0.439
5	1.313	0.0	0.436	0.453
6	1.329	0.0	0.449	0.466
7	1.391	0.0	0.483	0.500
8	1.446	0.0	0.503	0.520
9	1.497	0.0	0.521	0.538
10	1.545	0.0	0.536	0.553
11	1.591	0.0	0.547	0.564
12	1.746	0.0	0.578	0.595
13	1.882	0.0	0.601	0.617
14	2.004	0.0	0.623	0.639
15	2.115	0.0	0.644	0.660
16	2.218	0.0	0.661	0.677
17	2.404	0.0	0.690	0.706
18	2.570	0.0	0.717	0.733
19	2.721	0.0	0.741	0.757
20	2.860	0.0	0.760	0.776
21	2.989	0.0	0.775	0.791
22	3.188	0.0	0.801	0.816
23	3.370	0.0	0.825	0.840
24	3.537	0.0	0.848	0.861
25	3.694	0.0	0.867	0.880
26	3.841	0.0	0.885	0.896
27	3.979	0.0	0.901	0.912
28	4.111	0.0	0.916	0.926

Table 14

Streamline Data Downstream of Rotor Exit for Basic Flow No. 1

Streamline Number	r (inches)	V_θ/V_∞	V_x/V_∞	V_m/V_∞
1	0.583	0.364	0.376	0.386
2	0.625	0.344	0.399	0.409
3	0.662	0.328	0.419	0.429
4	0.695	0.316	0.438	0.448
5	0.726	0.306	0.455	0.465
6	0.754	0.298	0.470	0.481
7	0.852	0.280	0.523	0.533
8	0.932	0.274	0.563	0.573
9	1.001	0.270	0.598	0.608
10	1.062	0.266	0.627	0.637
11	1.118	0.264	0.652	0.662
12	1.293	0.260	0.726	0.735
13	1.435	0.259	0.784	0.793
14	1.555	0.258	0.833	0.482
15	1.661	0.255	0.873	0.882
16	1.757	0.249	0.902	0.911
17	1.929	0.226	0.933	0.942
18	2.084	0.201	0.947	0.956
19	2.225	0.181	0.960	0.969
20	2.357	0.165	0.972	0.980
21	2.480	0.148	0.974	0.983
22	2.676	0.113	0.951	0.960
23	2.861	0.087	0.937	0.945
24	3.035	0.078	0.958	0.967
25	3.197	0.067	0.967	0.976
26	3.354	0.041	0.919	0.927
27	3.515	0.005	0.826	0.832
28	3.678	0.000	0.829	0.836

Table 15

Final Outlet Angles for Basic Flow No. 2

r/R_R	β_2	δ_o	$\Delta\delta^*$	$\Delta\delta'$	$\Delta\delta_s$	β_2^*
0.26	49.0	2.6	9.6	3.4	-5.9	51.9
0.30	49.8	3.4	7.0	1.1	-3.2	55.9
0.40	52.7	4.7	4.0	2.2	-1.1	58.1
0.50	55.9	5.4	2.3	2.9	----	60.7
0.60	59.6	5.8	1.7	2.3	----	64.8
0.70	63.5	5.2	1.2	1.7	----	68.2
0.80	67.2	4.5	0.8	1.4	----	71.1
0.90	70.2	3.2	0.6	1.1	----	72.9
0.95	73.3	1.9	0.3	0.0	----	75.5

	Inlet Velocity Profile		Outlet Velocity Profile		
r/R_R	V_x/V_∞	β_1	V_x/V_∞	V_θ/V_∞	β_2^*
0.26	0.465	64.9	0.543	0.301	51.8
0.30	0.569	63.6	0.594	0.269	55.9
0.40	0.693	65.6	0.774	0.280	58.2
0.50	0.779	67.8	0.917	0.279	60.7
0.60	0.843	69.8	0.966	0.231	64.9
0.70	0.891	71.6	0.998	0.184	68.2
0.80	0.912	73.4	1.000	0.132	71.1
0.90	0.914	75.1	1.034	0.095	72.8
0.95	0.913	75.9	0.927	0.043	75.5

Table 16

Final Results for Basic Flow No. 3

r/R_R	β_2	δ_o	$\Delta\delta^*$	$\Delta\delta'$	$\Delta\delta_s$	β_2^*
0.26	49.0	2.5	9.0	2.9	-5.5	52.1
0.30	49.8	3.4	6.8	1.8	-2.9	55.3
0.40	52.7	4.6	4.0	2.2	-1.1	58.0
0.50	55.9	5.4	2.7	2.9	----	61.1
0.60	59.6	5.8	1.7	2.2	----	64.9
0.70	63.5	5.2	1.4	1.6	----	68.5
0.80	67.2	4.5	0.8	0.9	----	71.6
0.90	70.2	3.2	0.6	1.0	----	72.9
0.95	73.3	1.9	0.3	0.0	----	75.5

	Inlet Velocity Profile		Outlet Velocity Profile		
r/R_R	V_x/V_∞	β_1	V_x/V_∞	V_θ/V_∞	β_2^*
0.26	0.442	63.7	0.495	0.258	52.1
0.30	0.515	63.5	0.557	0.227	55.3
0.40	0.636	65.1	0.707	0.239	58.1
0.50	0.708	67.7	0.821	0.236	61.1
0.60	0.758	69.8	0.871	0.197	65.0
0.70	0.804	71.6	0.892	0.149	68.5
0.80	0.830	73.2	0.882	0.099	71.6
0.90	0.844	74.7	0.934	0.075	72.8
0.95	0.847	75.5	0.831	0.027	75.6

Table 17

Final Results for Basic Flow No. 4

r/R_R	β_2	δ_o	$\Delta\delta^*$	$\Delta\delta'$	$\Delta\delta_s$	β_2^*
0.26	49.0	2.5	8.7	1.2	-5.0	54.0
0.30	49.8	3.4	6.6	0.1	-3.2	56.5
0.40	52.7	4.6	4.1	2.9	-1.3	57.2
0.50	55.9	5.4	2.5	2.9	----	60.9
0.60	59.6	5.7	1.7	2.3	----	64.7
0.70	63.5	5.1	1.3	1.6	----	68.3
0.80	67.2	4.5	0.8	1.0	----	71.5
0.90	70.2	3.2	0.6	1.5	----	72.5
0.95	73.3	1.8	0.3	0.0	----	75.4

	Inlet Velocity Profile		Outlet Velocity Profile		
r/R_R	V_x/V_∞	β_1	V_x/V_∞	V_θ/V_∞	β_2^*
0.26	0.459	62.8	0.486	0.229	53.9
0.30	0.542	62.3	0.531	0.230	56.5
0.40	0.608	66.1	0.709	0.270	57.3
0.50	0.704	67.8	0.819	0.251	60.9
0.60	0.759	69.8	0.873	0.209	64.8
0.70	0.802	71.6	0.896	0.162	68.3
0.80	0.827	73.3	0.883	0.111	71.5
0.90	0.834	74.9	0.952	0.091	72.4
0.95	0.834	75.7	0.835	0.037	75.5

Table 18

Basic Flow Configurations

Basic Flow Nos.	Upstream Struts**	Upstream Screen	Flow Coefficient ϕ***	Rotor Cap
1	Without	Without	Design	Conical
2	Without	Without	0.9 Design	Conical
3	Without	With	Design	Conical
4	With	Without	Design	Conical
5	With	Without	1.1 Design	Conical
6	With	Without	0.9 Design	Conical

** The upstream struts consisted of four struts place of 0°, 90°, 180°, 270° on the surface.

*** The flow coefficient is defined as $\phi = \frac{V_\infty}{U_{TIP}}$.

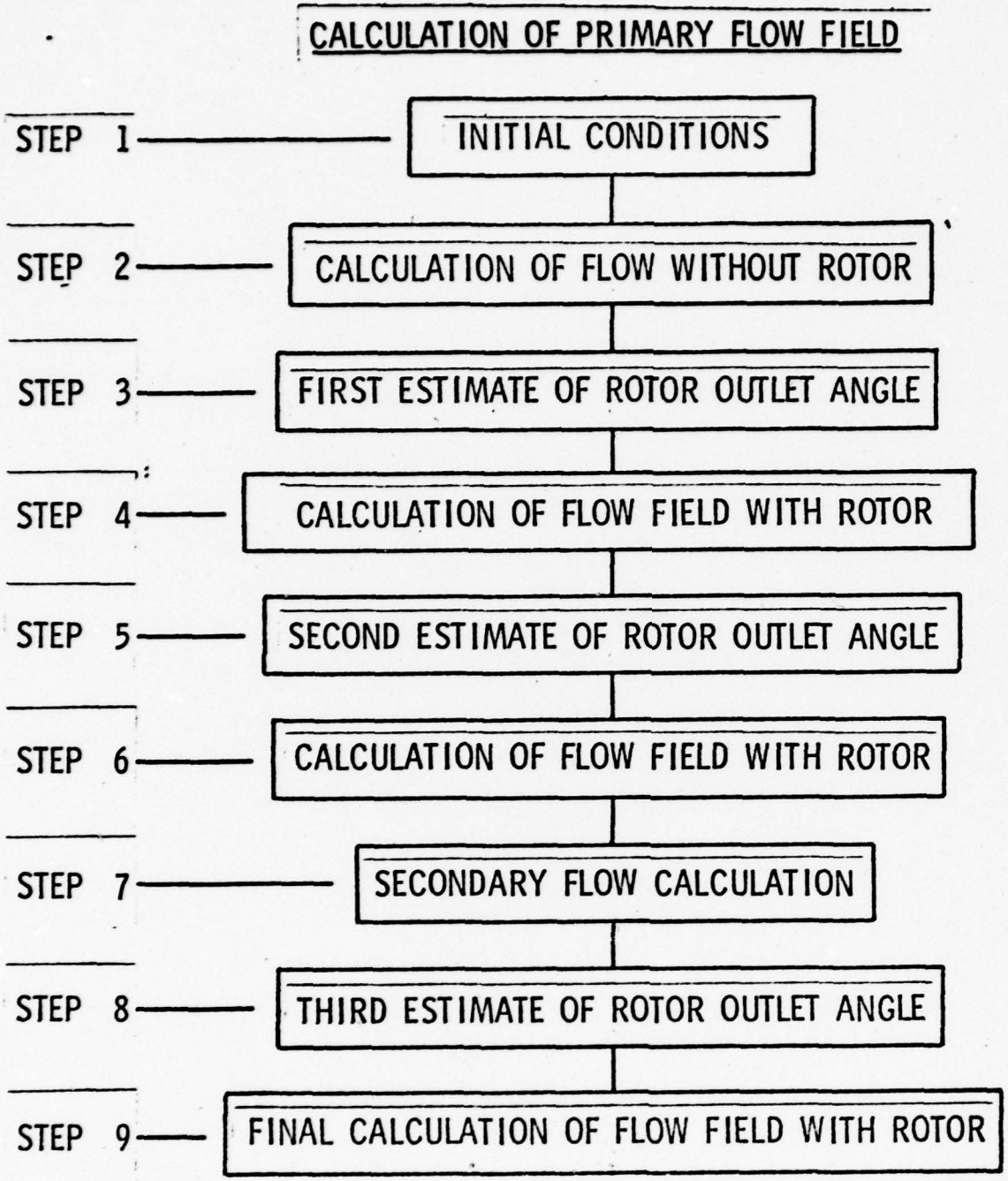

Figure 1 - Schematic of Calculation Procedure for Primary Flow Field

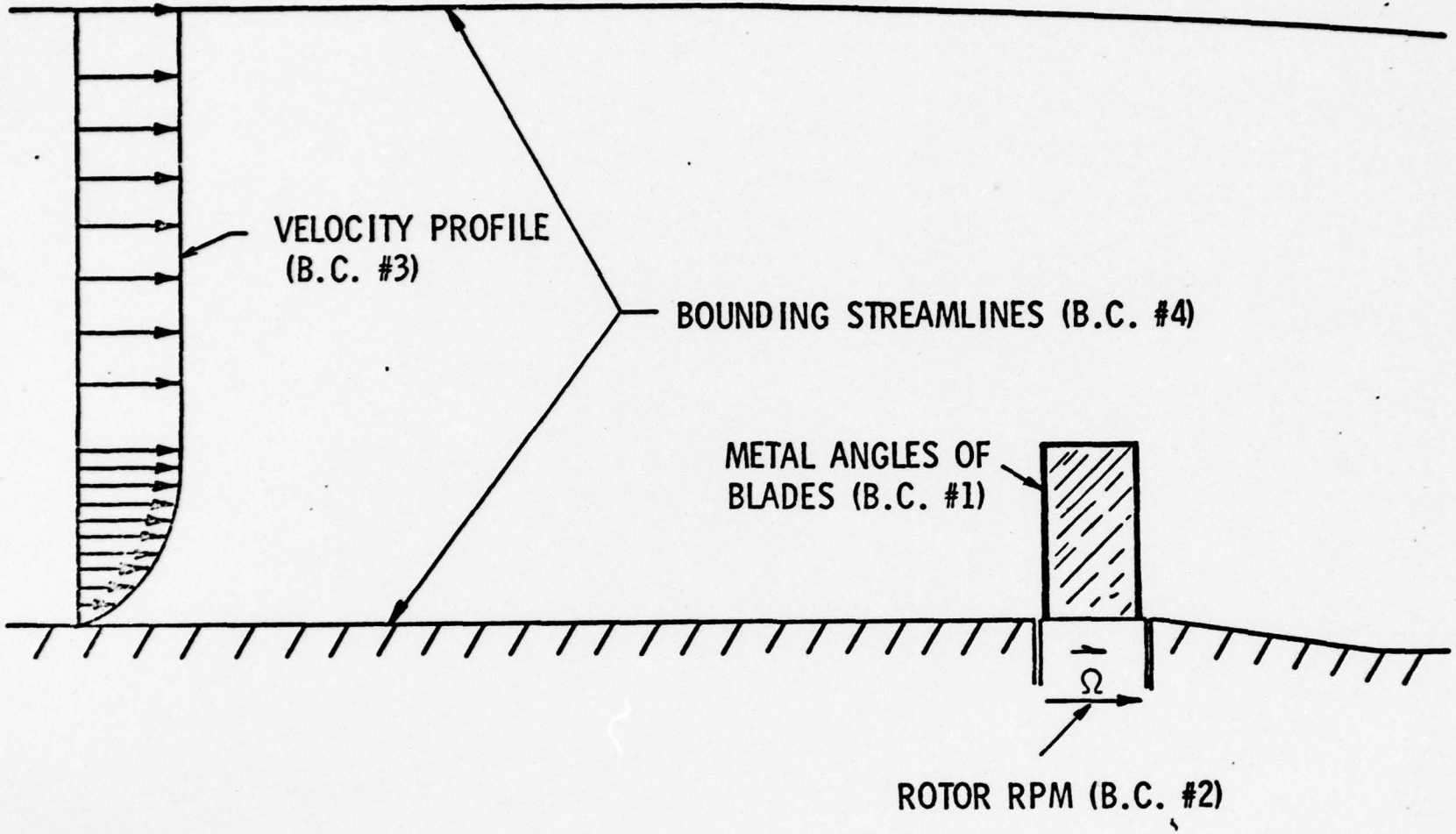

Figure 2 - Schematic of Boundary Conditions

11 May 1978
MLB:jep

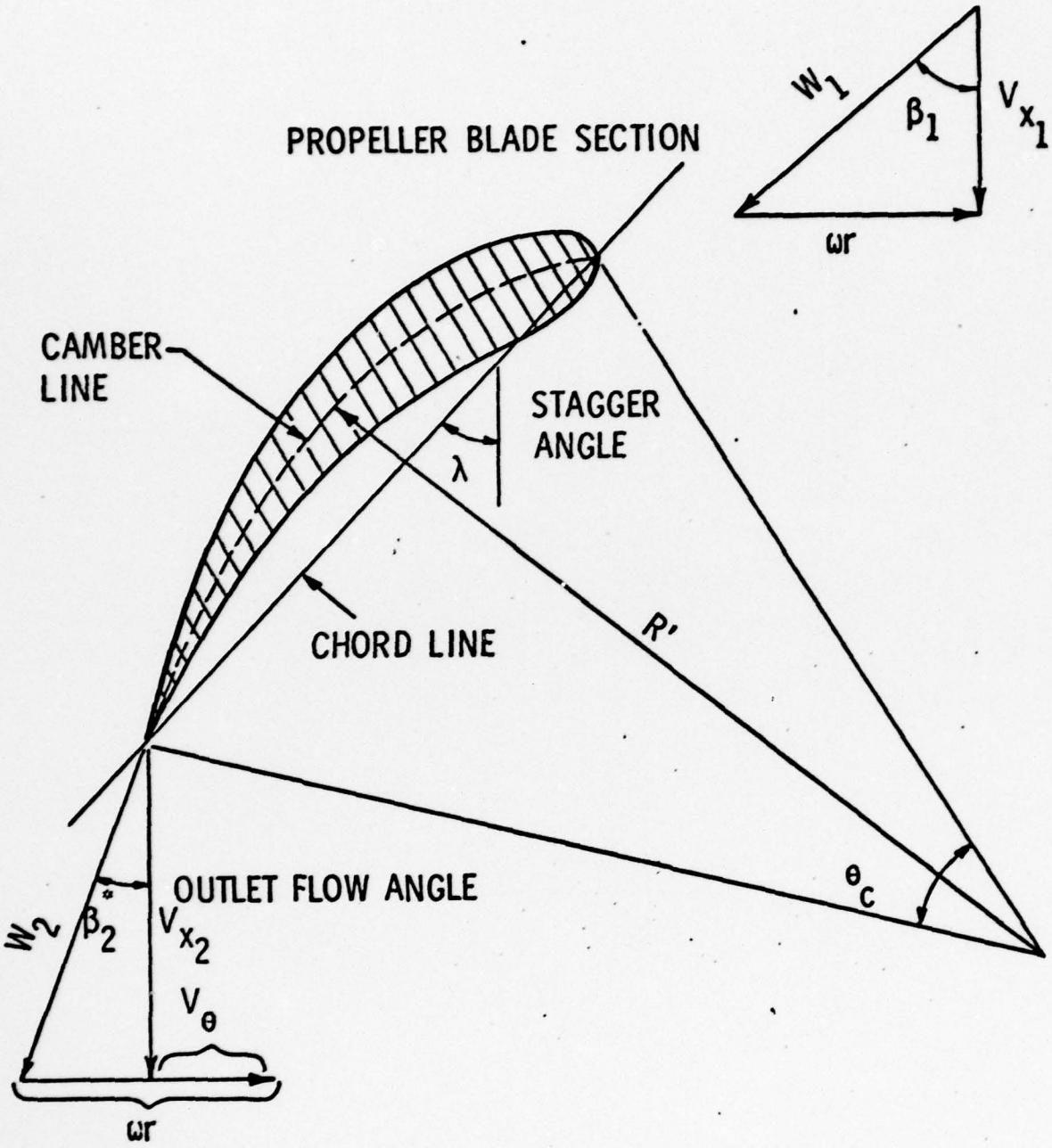

Figure 3 - Definition of Blade Angles

11 May 1978
MLB:jep

11 May 1978
MLB:jep

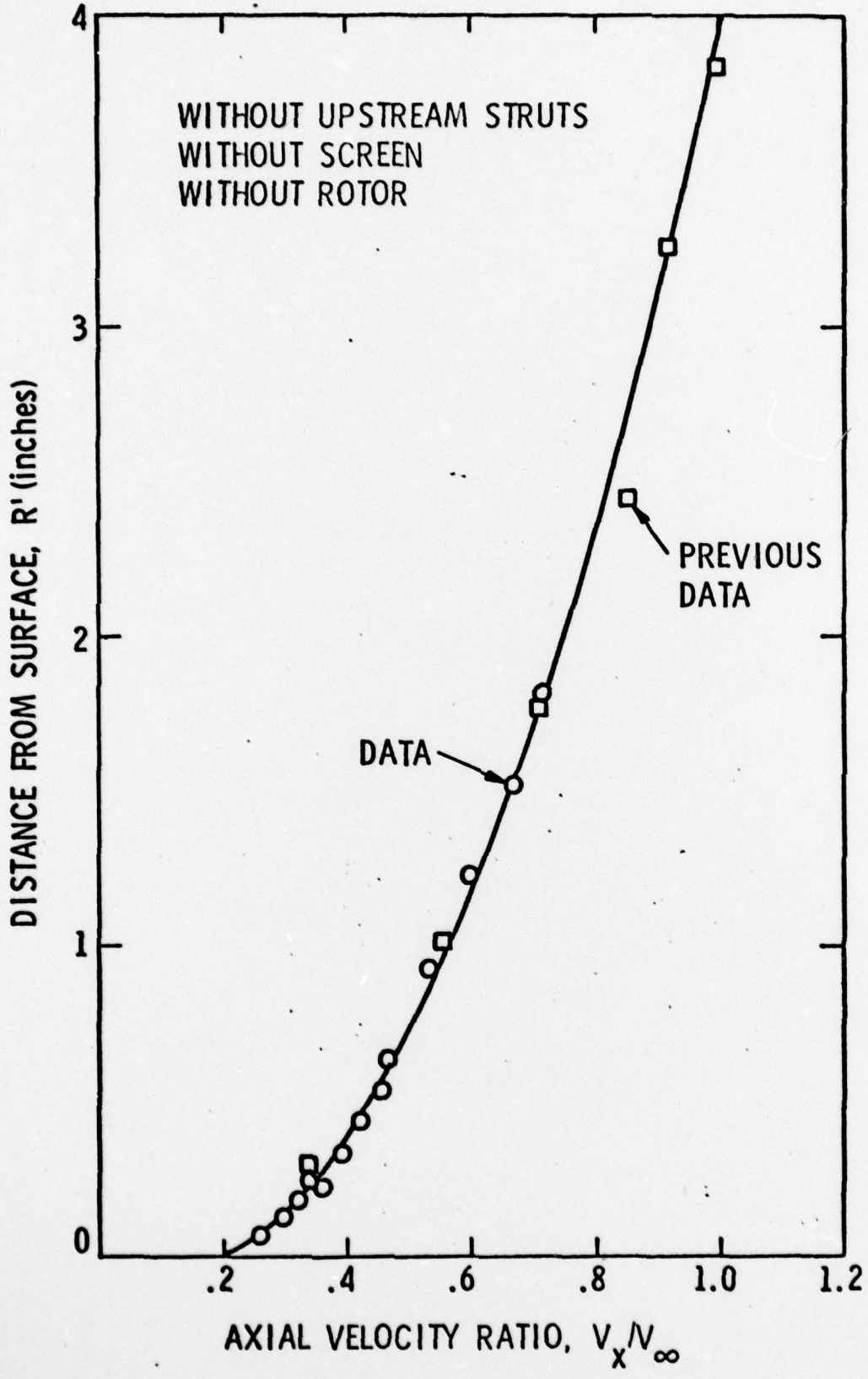

Figure 4 - Boundary Layer for Bare Body

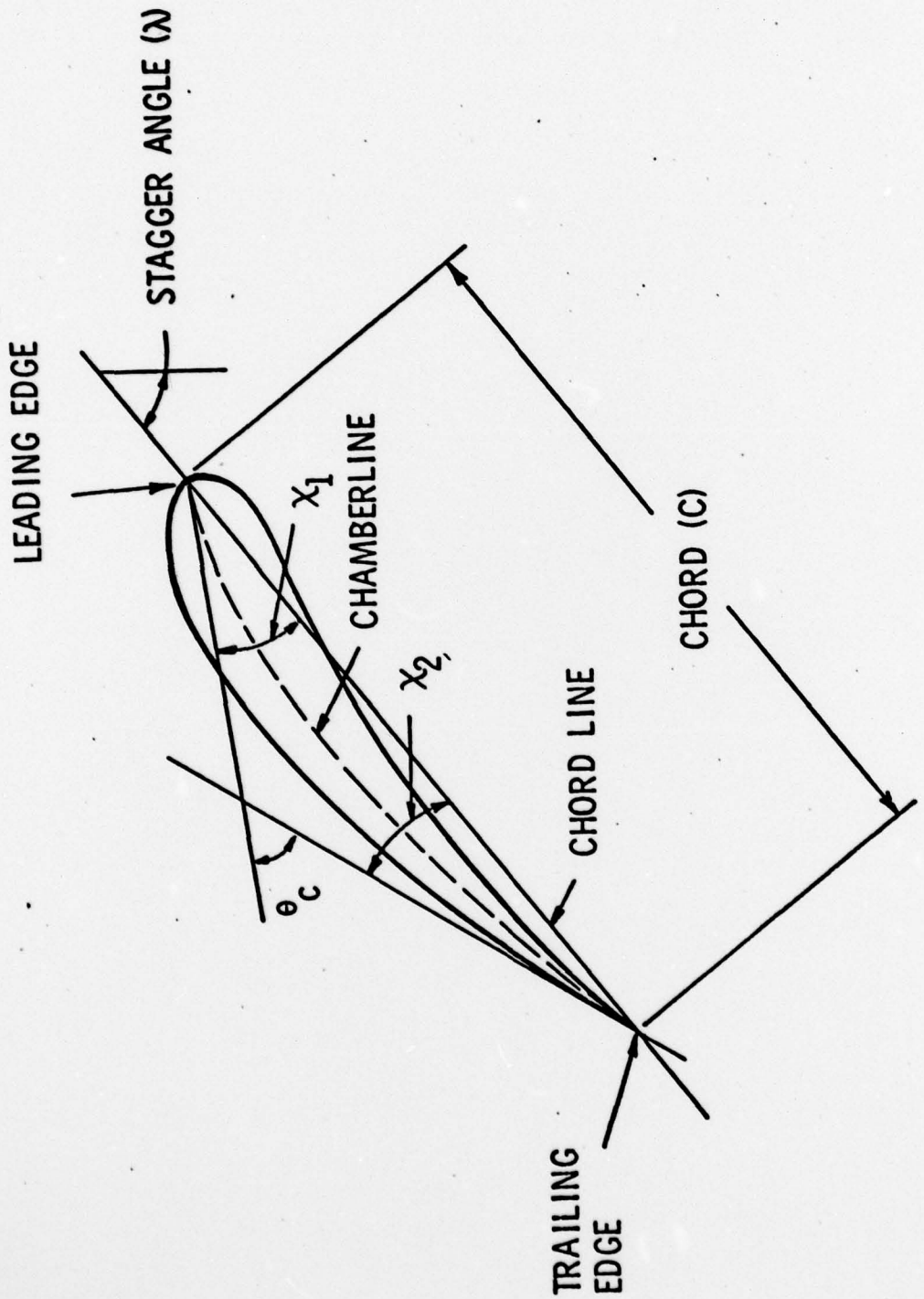

Figure 5 - Geometry of Blade Angles

11 May 1978
MLB:jep

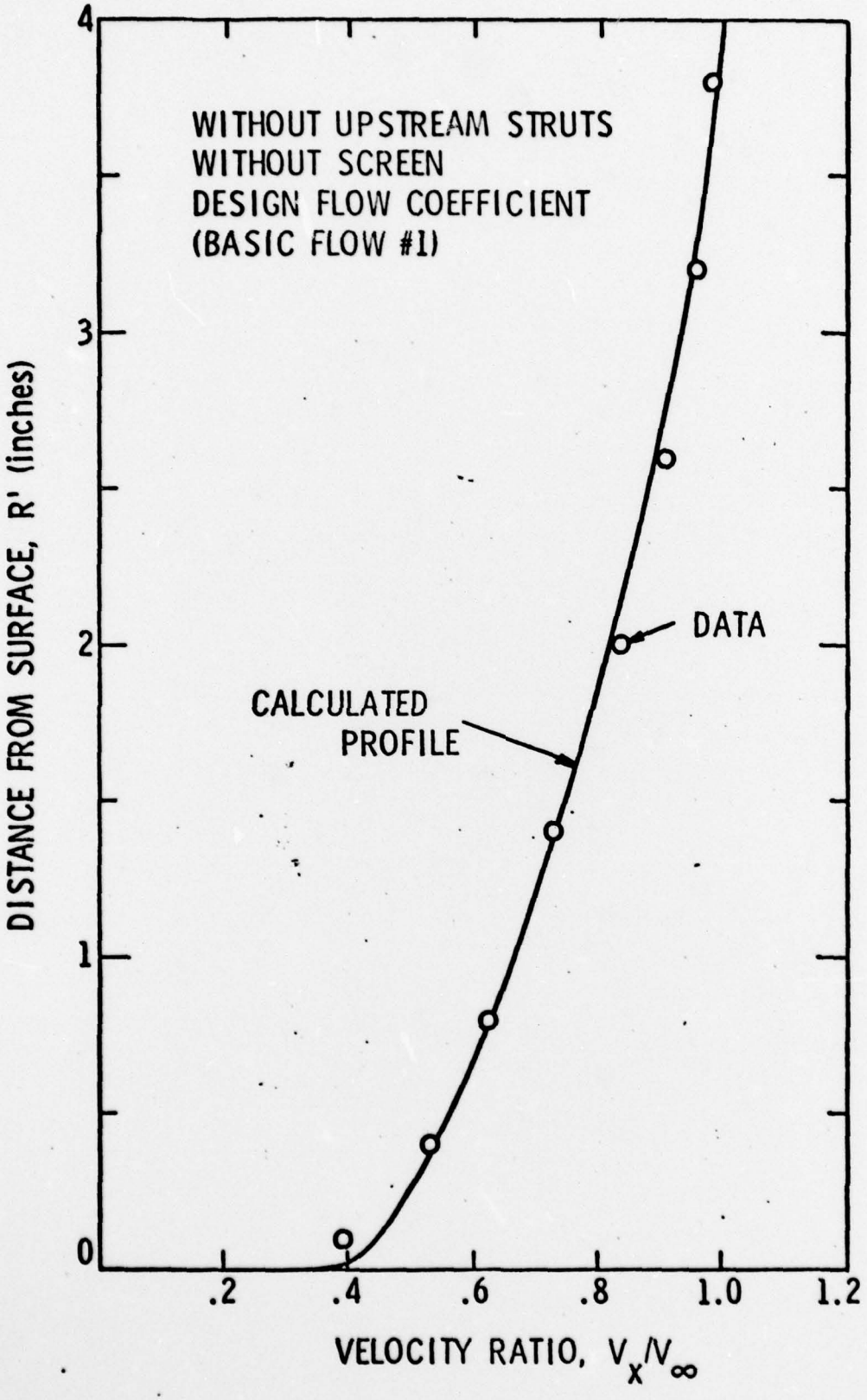

Figure 6 - Rotor Inlet Velocity Profiles for Basic Flow No. 1

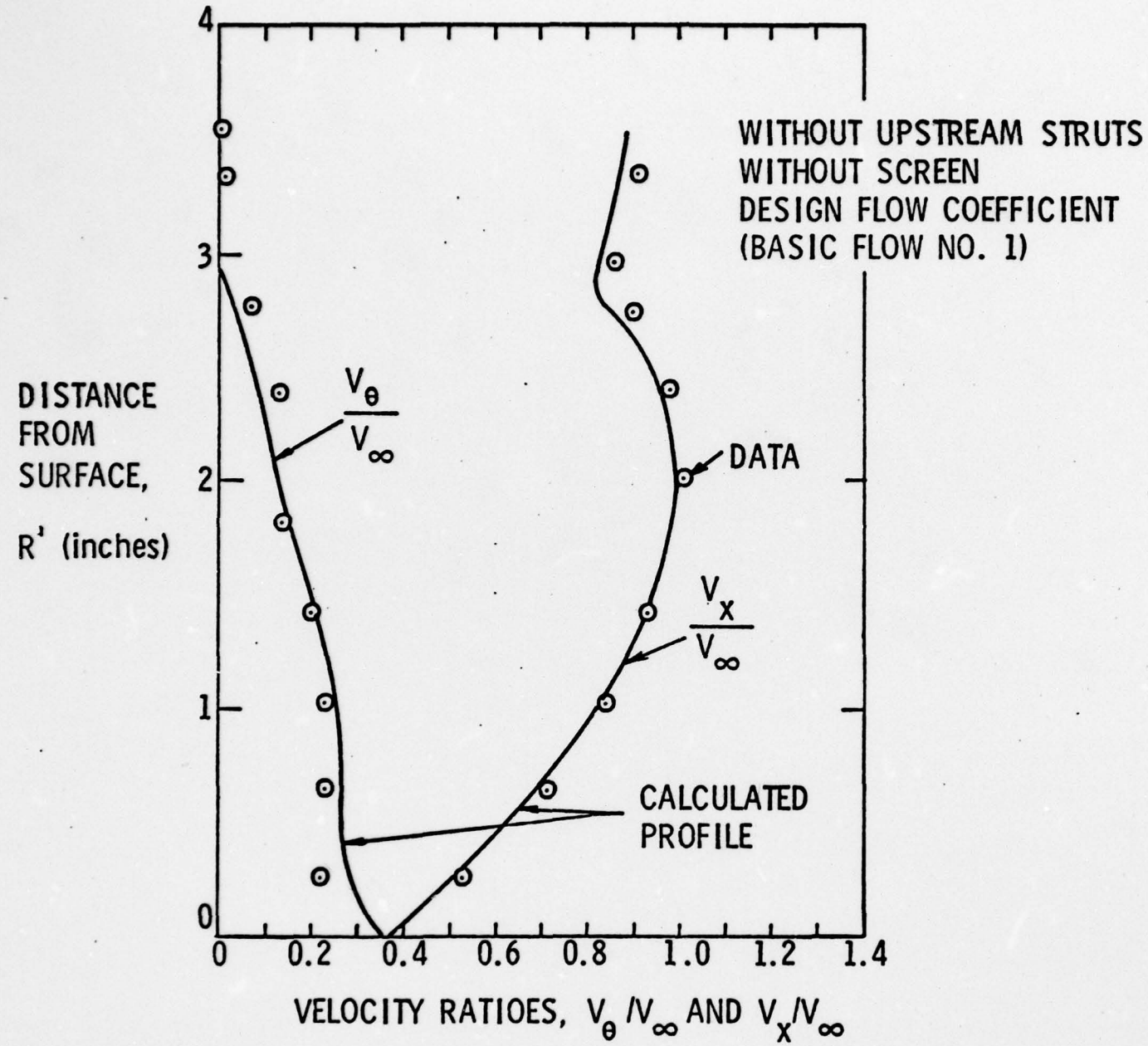

Figure 7 - Rotor Outlet Velocity Profiles for Basic Flow No. 1

11 May 1978
MLB:jep

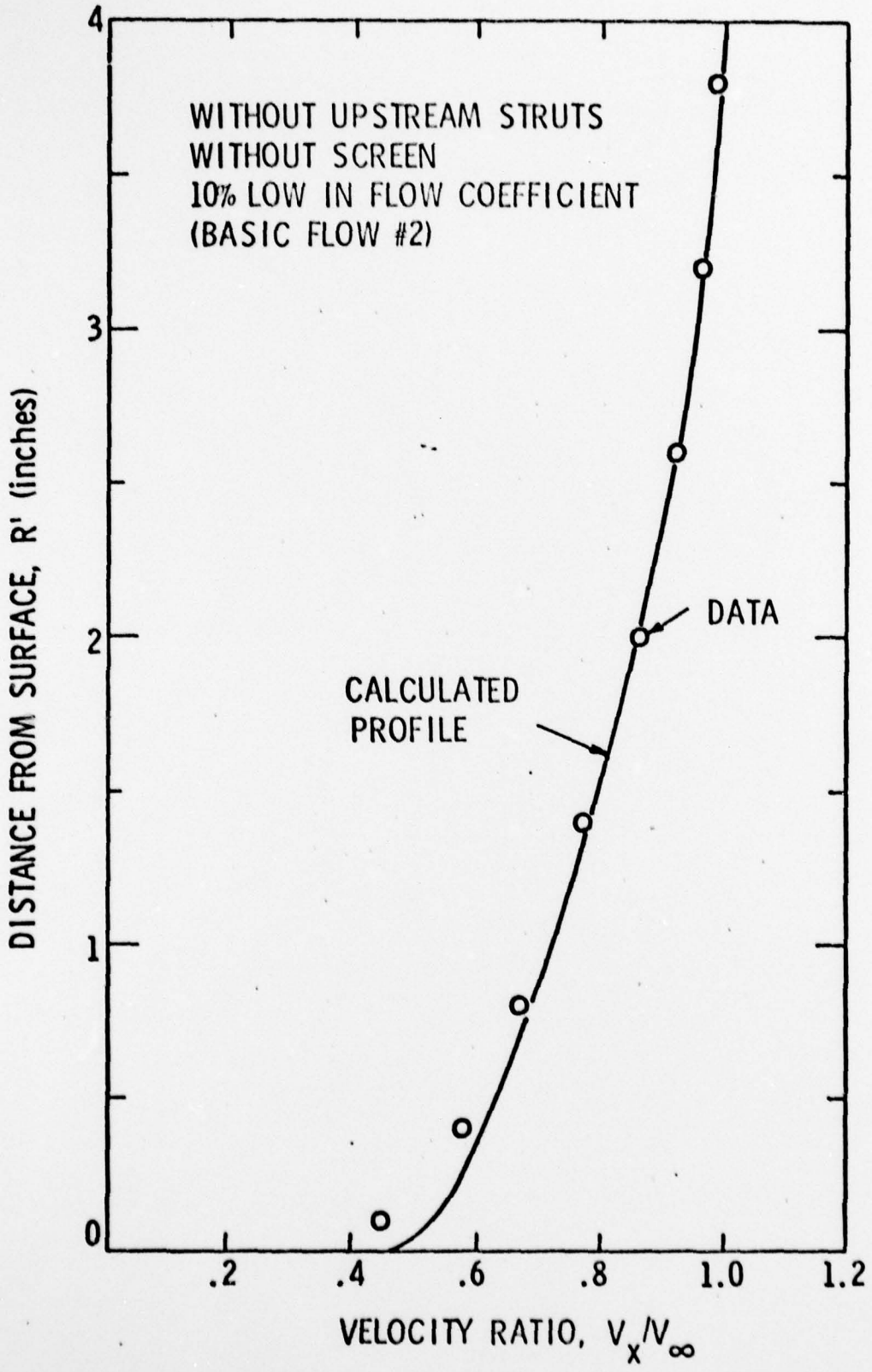

Figure 8 - Rotor Inlet Velocity Profiles for Basic Flow No. 2

11 May 1978
MLB:jep

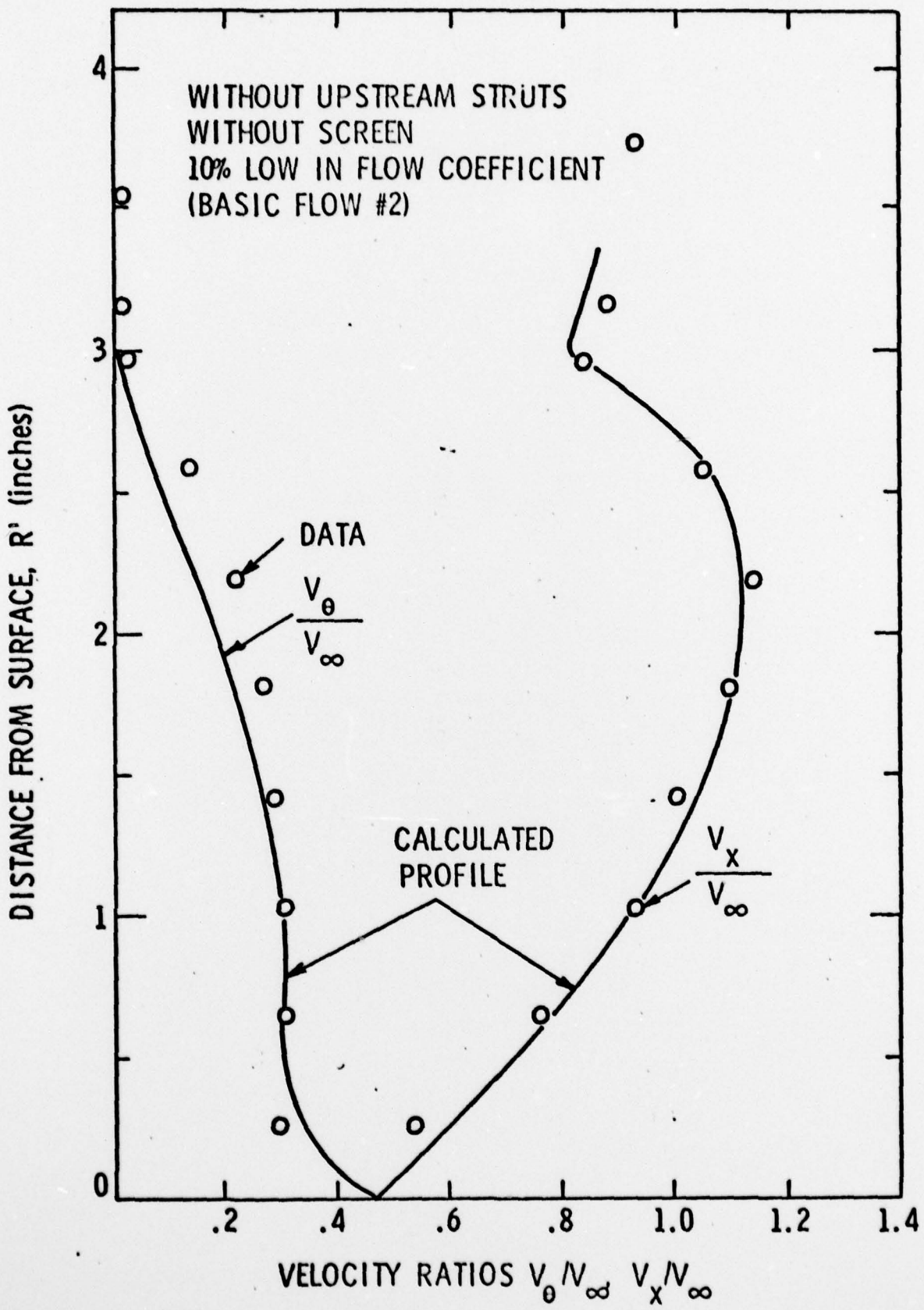

Figure 9 - Rotor Outlet Velocity Profiles for Basic Flow No. 2

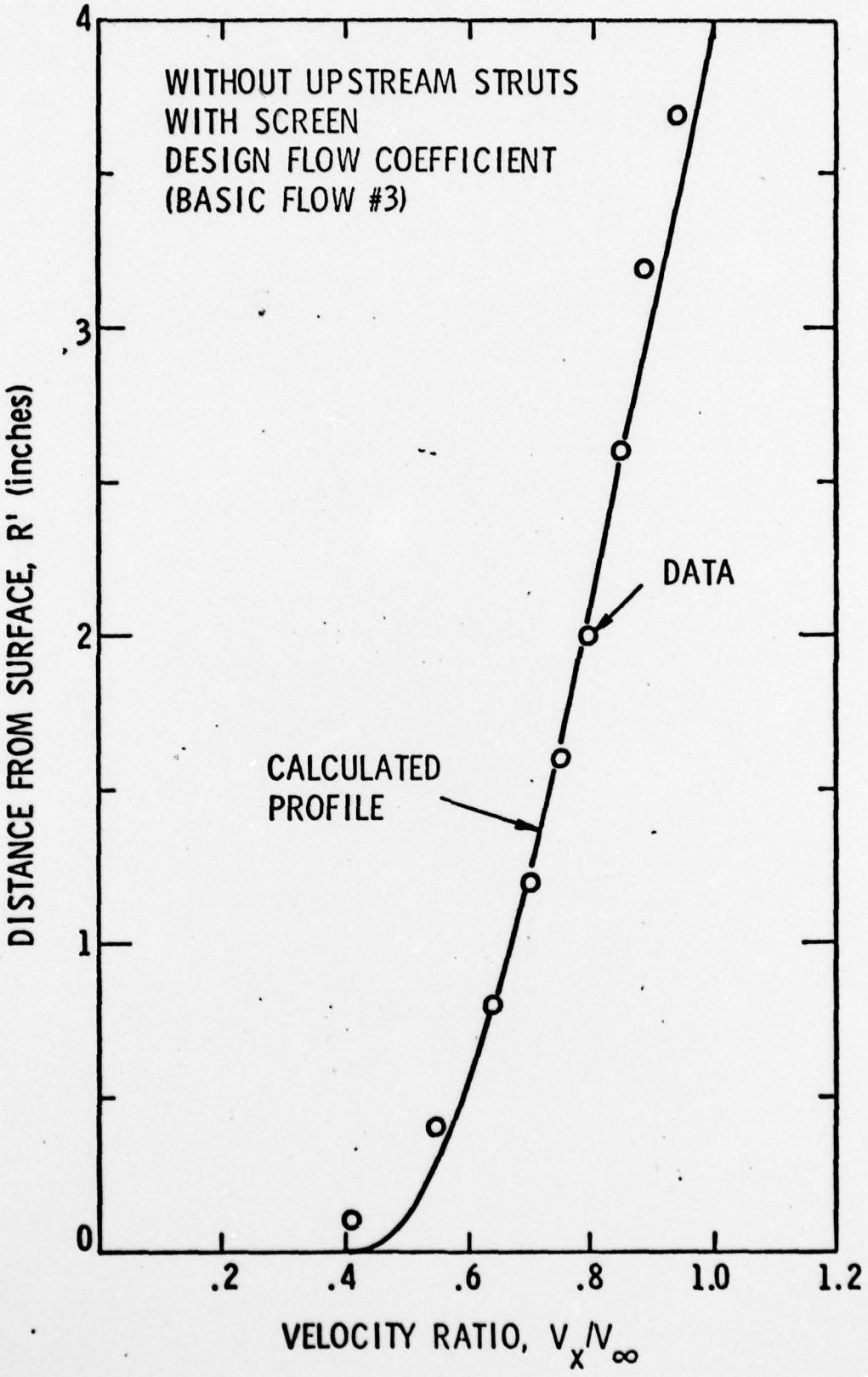

Figure 10 - Rotor Inlet Velocity Profiles for Basic Flow No. 3

11 May 1978
MLB:jep

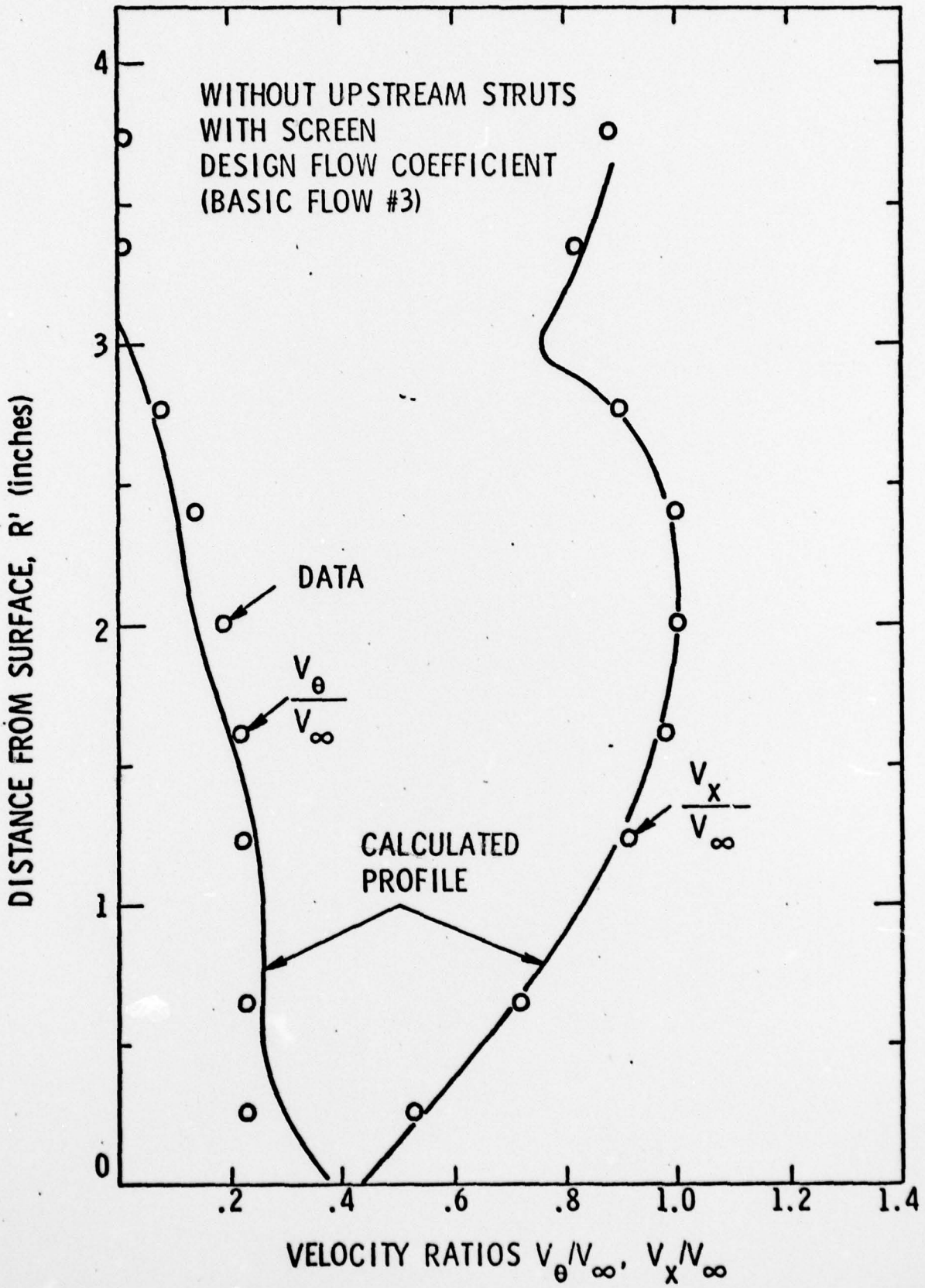

Figure 11 - Rotor Outlet Velocity Profiles for Basic Flow No. 3

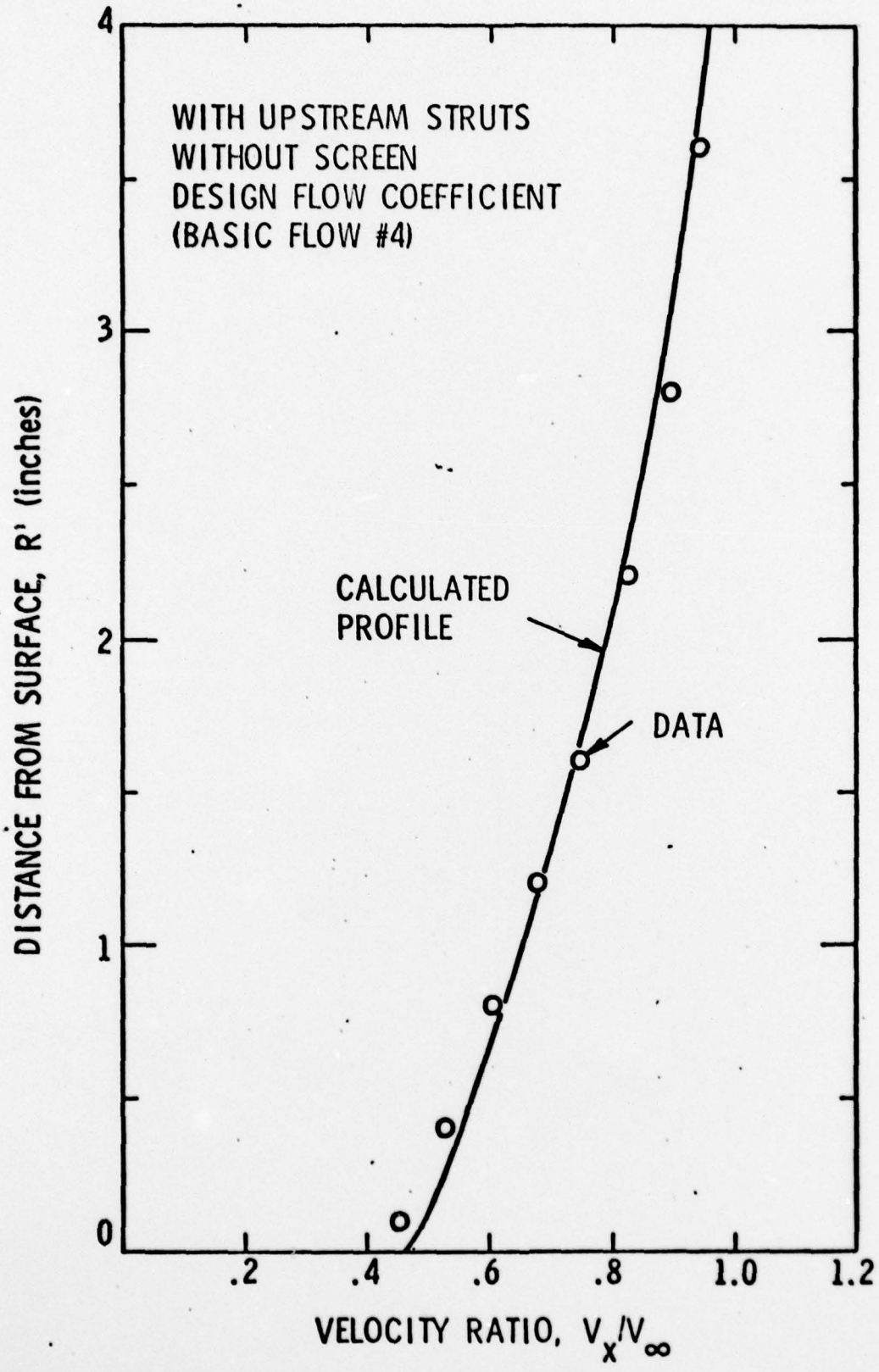

Figure 12 - Rotor Inlet Velocity Profiles for Basic Flow No. 4

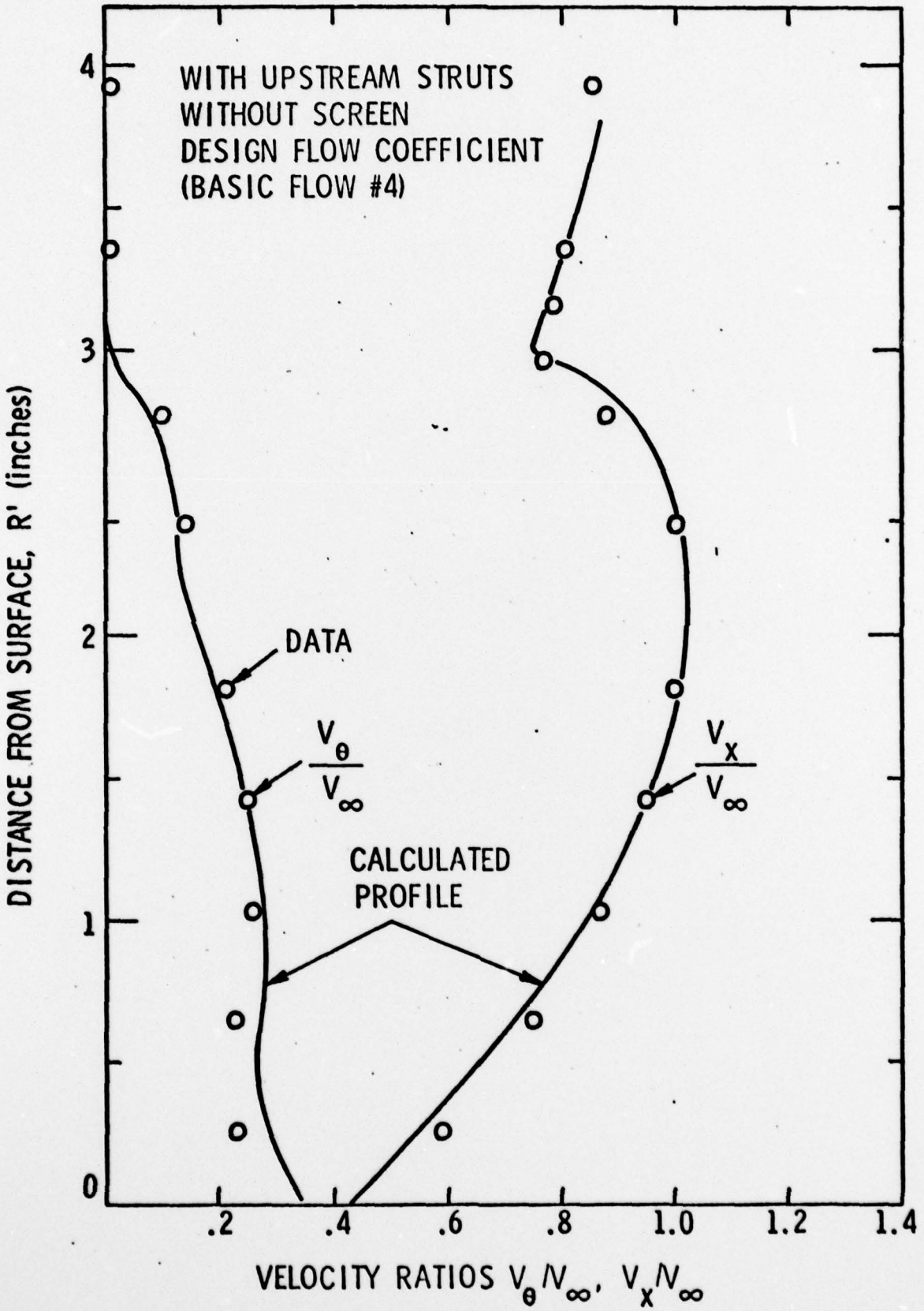

Figure 13 - Rotor Outlet Velocity Profiles for Basic Flow No. 4

11 May 1978
MLB:jep

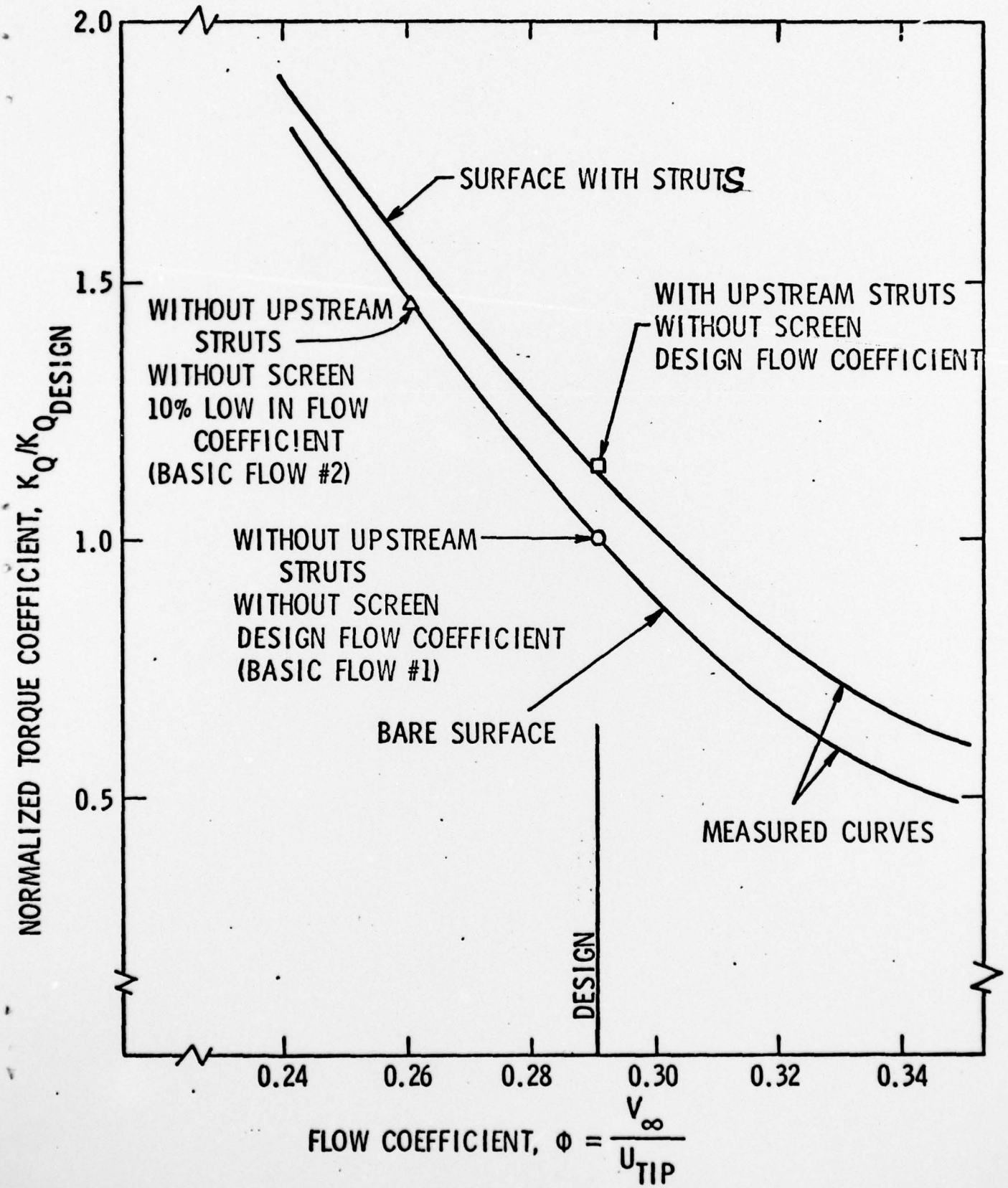

Figure 14 - Torque Coefficient for Rotor

DISTRIBUTION LIST FOR UNCLASSIFIED TM 78-161 by M. L. Billet, dated 11 May 1978

Commander
Naval Sea Systems Command
Department of the Navy
Washington, DC 20362
Attn: Library
Code NSEA-09G32
(Copy Nos. 1 and 2)

Naval Sea Systems Command
Attn: Code NSEA-0342
Copy Nos. 3 and 4)

Naval Sea Systems Command
Attn: T. E. Peirce
Code NSEA-0351
(Copy No. 5)

Naval Sea Systems Command
Attn: A. R. Paladino
Code NSEA-0372
(Copy No. 6)

Commanding Officer
Naval Underwater Systems Center
Newport, RI 02840
Attn: Library
Code LA15
(Copy No. 7)

Commanding Officer
Naval Ocean Systems Center
San Diego, CA 92152
Attn: Library
(Copy No. 8)

Naval Ocean Systems Center
Attn: J. W. Hoyt
Code 2501
(Copy No. 9)

Commander
Naval Surface Weapon Center
Silver Spring, MD 20910
Attn: Library
(Copy No. 10)

Commanding Officer and Director
David W. Taylor Naval Ship R&D Center
Department of the Navy
Bethesda, MD 20084
Attn: W. B. Morgan
Code 154
(Copy No. 11)

David W. Taylor Naval Ship R&D Center
Attn: Tech. Info. Lib.
Code 522.1
(Copy No. 12)

David W. Taylor Naval Ship R&D Center
Attn: M. Sevik
Code 19
(Copy No. 13)

David W. Taylor Naval Ship R&D Center
Attn: S. Crump
Code 1505
(Copy Nos. 14 - 33)

Defense Documentation Center
5010 Duke Street
Cameron Street
Alexandria, VA 22314
Copy Nos. 34 - 45)

Iowa Institute of Hydraulic Research
State University of Iowa
Iowa City, Iowa 52240
Attn: Director
(Copy No. 46)

Dr. Ralph Cooper
Office of Naval Research
Department of the Navy
800 N. Quincy Street
Arlington, VA 22217
(Copy No. 47)

Dr. B. Lakshminarayana
153-J Hammond Building
Department of Aerospace Engineering
The Pennsylvania State University
University Park, PA 16802
(Copy No. 48)

APPLIED RESEARCH LABORATORY
The Pennsylvania State University
Post Office Box 30
State College, PA 16801
Attn: Dr. J. W. Holl
(Copy Nos. 49 - 54)

APPLIED RESEARCH LABORATORY
Attn: M. L. Billet
(Copy No. 55)

DISTRIBUTION LIST FOR UNCLASSIFIED TM 78-161 by M. L. Billet, dated 11 May 1978

APPLIED RESEARCH LABORATORY
Attn: R. E. Henderson
(Copy No. 56)

APPLIED RESEARCH LABORATORY
Attn: A. L. Treaster
(Copy No. 57)

APPLIED RESEARCH LABORATORY
Attn: B. E. Robbins
(Copy No. 58)

APPLIED RESEARCH LABORATORY
Attn: D. E. Thompson
(Copy No. 59)

APPLIED RESEARCH LABORATORY
Attn: D. R. Stinebring
(Copy No. 60)

APPLIED RESEARCH LABORATORY
Attn: GTWT Library
(Copy No. 61)